

Stellar Population in LLAGN.II: STIS observations ¹

Rosa M. González Delgado¹, Roberto Cid Fernandes², Enrique Pérez¹, Lucimara P. Martins^{3,7}, Thaisa Storchi-Bergmann⁴, Henrique Schmitt^{5,8}, Timothy Heckman^{6,9}, & Claus Leitherer³

(1) Instituto de Astrofísica de Andalucía (CSIC), P.O. Box 3004, 18080 Granada, Spain
(rosa@iaa.es; eperez@iaa.es)

(2) Depto. de Física-CFM, Universidade Federal de Santa Catarina, C.P. 476, 88040-900, Florianópolis, SC, Brazil (cid@astro.ufsc.br)

(3) Space Telescope Institute, 3700 San Martin Drive, Baltimore, MD 21218, USA
(martins@stsci.edu; leitherer@stsci.edu)

(4) National Radio Astronomy Observatory, PO Box 0, Socorro, NM 87801
(hschmitt@nrao.edu)

(5) Instituto de Física, Universidad Federal do Rio Grande do Sul, C.P. 15001, 91501-970, Poto Alegre, RS, Brazil (thaisa@if.ufrgs.br)

(6) Department of Physics & Astronomy, JHU, Baltimore, MD 21218
(heckman@pha.jhu.edu)

(7) Intituto de Astronomia, Geofísica e Ciências Atmosféricas, 05508-900 Sao Paulo, Brazil

ABSTRACT

We present a study of the stellar population in Low Luminosity Active Galactic Nuclei (LLAGN). Our goal is to search for spectroscopic signatures of young and intermediate age stars, and to investigate their relationship with the ionization mechanism in LLAGN. The method used is based on the stellar population synthesis of the optical continuum of the innermost (20-100 pc) regions in these galaxies. For this purpose, we have collected high spatial resolution optical (2900-5700 Å) STIS spectra of 28 nearby LLAGN that are available in the *Hubble Space Telescope* archive. The analysis of these data is compared with a similar analysis also presented here for 51 ground-based spectra of LLAGN. Our main findings

⁸Jansky Fellow

⁹Also Adjunct Astronomer at STScI

are: (1) No features due to Wolf-Rayet stars were convincingly detected in the STIS spectra. (2) Young stars contribute very little to the optical continuum in the ground-based aperture. However, the fraction of light provided by these stars is higher than 10% in most of the weak-[OI] ($[\text{OI}]/\text{H}\alpha \leq 0.25$) LLAGN STIS spectra. (3) Intermediate age stars contribute significantly to the optical continuum of these nuclei. This population is more frequent in objects with weak than with strong [OI]. Weak-[OI] LLAGN that have young stars stand out for their intermediate age population. (4) Most of the strong-[OI] LLAGN have predominantly old stellar population. A few of these objects also show a feature-less continuum that contributes significantly to the optical continuum. These results suggest that young and intermediate age stars do not play a significant role in the ionization of LLAGN with strong [OI]. However, the ionization in weak-[OI] LLAGN with young and/or intermediate age population could be due to stellar processes. A comparison of the properties of these objects with Seyfert 2 galaxies that harbor a nuclear starburst, suggests that weak-[OI] LLAGN are the lower luminosity counterparts of the Seyfert 2 composite nuclei.

Subject headings: galaxies: active – galaxies: nuclei – galaxies: stellar content – galaxies: starburst

1. Introduction

Low-Luminosity Active Galactic Nuclei (LLAGN) constitute a sizeable fraction of the nearby AGN population. These include low-luminosity Seyferts, low-ionization nuclear emission-line regions (LINERs), and transition-type objects (TOs) whose properties are in between classical LINERs and HII nuclei. LLAGN comprise about 1/3 of all bright galaxies ($B_T \leq 12.5$) and are the most common type of AGNs (Ho, Filippenko & Sargent 1997a; hereafter HFS97).

TOs could constitute a rather mixed phenomena as suggested by the several excitation mechanisms that have been proposed to explain the origin of their energy source. Among

¹Based on observations with the NASA/ESA *Hubble Space Telescope*, obtained at the Space Telescope Science Institute, which is operated by the Association of universities for Research in Astronomy, Inc., under NASA contract NAS 5-26555. Based on observations made with the Nordic Optical Telescope, operated on the island of La Palma jointly by Denmark, Finland, Iceland, Norway, and Sweden, in the Spanish Observatorio del Roque de los Muchachos of the Instituto de Astrofísica de Canarias.

these mechanisms are shocks, photoionisation by a non-stellar UV/X-ray continuum (AGN), and photoionisation by hot stars (see e.g. review by Filippenko 1996). The possibility that some LINERs (as well as Seyferts) might be photoionised by hot stars has been suggested by several authors (e.g. Stasińska 1984, Filippenko & Terlevich 1992, Shields 1992). These hot stars could be the product of the evolution of massive stars (the so-called *warmers* proposed by Terlevich & Melnick 1985) or of intermediate mass stars (the post-AGB stars investigated by Binette et al. 1994 by Taniguchi, Shioya, & Murayama 2000).

The massive star scenario has been reexamined by Barth & Shields (2000), using detailed starburst plus photoionisation modeling with evolutionary stellar synthesis models. These authors showed that the TOs properties can be reproduced by short stellar bursts with ages of $\sim 3\text{-}6$ Myr, when the ionizing continuum is dominated by emission from Wolf-Rayet (WR) stars. More recent photoionization models with updated Starburst99 (Smith, Norris, & Crowther 2002), which include new blanketed WR and O atmospheres, are not able to reproduce the typical TOs emission line ratios (González Delgado et al 2003).

There is further evidence in favor of the starburst scenario, coming from the detection of stellar wind lines in the ultraviolet spectra of some weak-[OI] LINERs and TOs (Maoz et al 1998; Colina et al 2002). In fact, similar spectroscopic features detected in Seyfert 2 galaxies are interpreted as due to a few Myr old nuclear starbursts (Heckman et al 1997; González Delgado et al 1998).

About 20% of LLAGN in the catalogue of HFS97 required a broad component to fit the $H\alpha$ emission (type 1 LINERs; Ho et al 1997b). Some of these objects show double-peaked H lines (Storchi-Bergmann et al 1997; Shields et al 2000; Ho et al 2000). In addition, recent X-ray observations of LLAGN confirm that some objects are at the low-luminosity end of the AGN phenomenon, and that they are powered by an accreting black-hole (BH) (Terasima, Ho, Ptak & 2000; Ho et al 2001).

Furthermore, recent high spatial resolution UV (Colina et al 2002) and Chandra (Jiménez-Bailón et al 2003) observations of the LLAGN NGC 4303 shows that a super-stellar cluster (SSC) and a BH accreting with low radiative efficiency coexist within the inner few pcs from the nucleus.

Considering the diversity of excitation mechanisms that can explain the emission line spectrum of LLAGN, we have started a project to examine the central stellar population in these objects, with the aim of finding clues about their physical origin and energy source. With this goal, we have carried out optical (3500–5500 Å) spectroscopic observations of LLAGN to: (1) search for the presence of the broad WR bump at the blue optical range (a blend of broad He II $\lambda 4686$, N III $\lambda 4640$ and C IV $\lambda 4650$); (2) detect the absorption lines of

HeI and the high order HI Balmer series (HOBLs); (3) characterize their stellar populations. The WR bump probes the presence of very young stars (few Myr old), while HeI and HOBLs probe the young (10–50 Myr) and intermediate (100–1000 Myr) age stars (González Delgado, Leitherer, & Heckman 1999). In addition, this spectral range contains many metallic stellar lines typical of old and intermediate age populations.

In a companion paper (Cid Fernandes et al. 2003a, hereafter Paper I), we have presented the data and an empirical correlation between the stellar lines and the emission lines in LLAGN, in particular the [OI]/H α line ratio. Our main findings from Paper I are: (1) No features due to WR stars are convincingly detected, implying that massive stars contribute very little to the optical light. This happens even in the few cases where young stars are known to dominate the UV emission. (2) HOBLs, on the other hand, are detected in 40% of the sample. These lines are absent in most strong-[OI] LLAGN, but they are detected in about 50% of the weak-[OI] LLAGN, defined as TOs and LINERs with [OI]/H α \leq 0.25. In fact, \sim 90% of nuclei exhibiting HOBLs are weak-[OI] emitters.

The analysis in Paper I was carried out entirely in empirical terms, investigating connections between observed quantities. In this paper we present a stellar population synthesis analysis of the nuclear spectra of these objects. Because our results may be affected by the spatial resolution of the ground-based observations, we also present here the analysis of 28 LLAGN observed at optical wavelengths with the Space Telescope Imaging Spectrograph (STIS) on board the Hubble Space Telescope (HST). The high spatial resolution provided by HST+STIS may be crucial to spatially-isolate the light from a central compact source or different circumnuclear star forming knots from the underlying light emitted by the old stars in the inner bulge of these galaxies.

Another major goal of this study is to investigate the low luminosity end of the “Starburst-AGN connection”. Powerful circumnuclear starbursts are present in 30–50% of type 2 Seyferts (Cid Fernandes et al. 2001a and references therein). The statistics are not clear for type 1 Seyferts due to the difficulty in spotting circumnuclear starbursts against the bright nucleus (which is conveniently obscured in Seyfert 2s), but if unification is correct the fraction of starburst+AGN composites should be similar in Seyfert 1s and 2s. If LINERs are just “mini-Seyferts”, one would naively expect to find circumnuclear starbursts in about 30–50% of them. Different incidence rates could be due to evolutionary effects, which, if present, should also be detected in a comparative stellar population analysis of Seyfert 2s and LINERs.

This paper is organized as follows: In section 2 we describe the sample and the STIS observations. Section 3 presents the STIS spectra and measurements of their properties. An empirical population synthesis (EPS) analysis of the whole sample (ground-based + STIS)

is presented in section 4. The results of this analysis are discussed in section 5, where we investigate the connection between the inferred stellar populations and emission line properties, compare our results with those obtained for Seyfert 2s and Starburst galaxies, and speculate on possible evolutionary scenarios. Finally, section 6 summarizes our conclusions.

2. Observations and data reduction

2.1. Galaxy Sample

Our sample of LLAGN was drawn entirely from the HFS97 catalogue because it is the most complete and homogeneous survey of LINERs and TOs available for the local universe. In addition to the galaxies presented in Paper I, we have selected LLAGN observed with STIS in the 2900–5700 Å spectral range. Spectra of 32 LLAGN are available in the HST archive, of which 28 galaxies (17 TOs and 11 LINERs according to the classification of HFS) are suitable for a stellar population analysis. Eight of these TOs have also been observed from the ground by us. These data are complemented with STIS spectra of four galaxies classified by HFS as HII nuclei, plus NGC 1023, a non-active galaxy. Most of these observations are from proposals number 8607 (P.I. L.C. Ho) and 7361 (P.I. H-W. Rix). These projects include 24 nearby early type (S0–Sb) galaxies and 15 TOs from the HFS97 catalogue which are closer than 17 Mpc and have emission lines with fluxes larger than 10^{-15} erg s $^{-1}$ cm $^{-2}$ Å $^{-1}$ in a 2×4 arcsec nuclear aperture. Observations of NGC 1023, NGC 3507, NGC 3998, and NGC 4261 are from proposals 7566 (P.I. R. Green), 7357 (P.I. L.C. Ho), 8839 (P.I. L. Dressel) and 8236 (P.I. S. Baum), respectively. Properties of these objects are listed in Table 1.

This collection plus data from Paper I increases the sample analyzed here to 33 TOs and 40 LINERs, which represents 49% of the TOs and 42% of the LINERs in the HFS97 sample. If we adopt a slightly different classification criterium for LLAGN, as we did in Paper I, placing the dividing line between the two subtypes at $[\text{OI}]/\text{H}\alpha=0.25$, our sample comprises 24 strong-[OI] and 47 weak-[OI] LLAGN, corresponding to 43% and 44% of these types of galaxies in the HFS97 sample. Morphological type and distance distributions are presented and compared with the full HFS97 sample in Figure 1. Our sample has the same median morphological type that the HFS97 sample; S0 and Sab for strong and weak-[OI] LLAGN, respectively. With respect to the distance, the median in our sample is 17 Mpc and 23 Mpc for weak-[OI] and strong-[OI] LLAGN, respectively. The corresponding values in the HFS sample are 20 Mpc and 22 Mpc.

2.2. Observations

The observations were obtained with the STIS/CCD detector with a 52×0.2 arcsec slit (except for NGC 3507, which was observed with a 0.5 arcsec slit) and the G430L grating. The spectra cover the wavelength range 2900–5700 Å with a dispersion of 2.7 Å/pixel, giving a minimum FWHM spectral resolution of ~ 4 Å for point sources and up to ~ 11 Å for extended sources. After an initial acquisition exposure of a few seconds through the optical long-pass filter, the slit was placed across each nucleus at a randomly oriented position angle. The CCD spatial scale is 0.05 arcsec/pixel. Observations from proposals 8607 and 8236 were binned every two pixels, yielding a spatial sampling of 0.1 arcsec.

The data were calibrated with the standard STScI pipeline, meaning that the spectra were bias and dark subtracted, flat fielded, cleaned of cosmic rays, corrected for geometrical distortion and flux calibrated. The total integration time was splitted in two or more individual exposures. In some objects, the telescope was offset by several pixels along the slit direction between repeated exposures to aid in the removal of hot pixels. If there are more than two exposures of the same object, the median frame was obtained. For those galaxies with two individual exposures, we combined the 2D spectra using a statistical differencing technique similar to that used by Pogge & Martini (2002) for WFPC2 images. The technique consists in obtaining for each individual exposure a mask frame containing only the hot pixels and cosmic-ray hits, which is then subtracted from the original spectrum. The mask is obtained as follows. First, for each pair of exposures, a difference spectrum is formed by subtracting one spectrum in the pair from the other. The resulting frames consist mainly of positive and negative cosmic-rays and hot pixels. A pair of mask frames is formed by separating the remaining positive and negative pixels, setting all the pixels within \pm a few σ of the mean residual background level on the difference spectrum to zero. This technique works well when the pair of original spectra have similar spatial distribution along the slit, and background.

All the spectra have been treated as extended continuum sources when converting from surface brightness units in the two-dimensional frames to flux units ($\text{erg s}^{-1} \text{cm}^{-2} \text{Å}^{-1}$). Finally, the spectra have been corrected for redshift assuming the heliocentric radial velocities listed in Table 1.

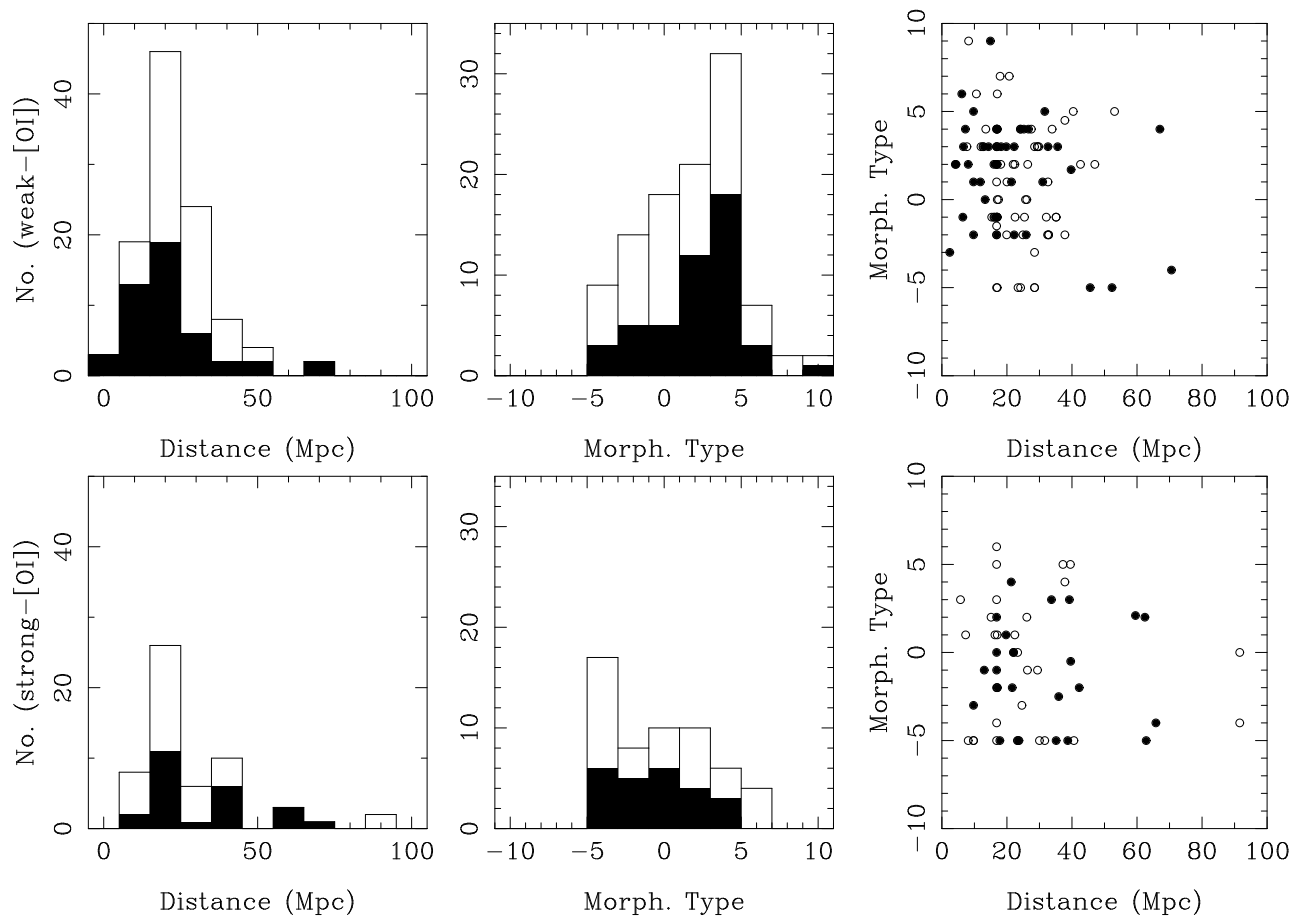


Fig. 1.— Distance and morphological type distributions for the strong-[OI] (lower panel) and weak-[OI] (upper panel) LLAGN in the HFS97 sample. Filled areas in the histograms indicate the sample analyzed here.

Table 1. LLAGN with archival STIS/CCD (G430L) spectra

Name	Type	Morph	v km/s	distance Mpc	1 arcsec pc ²	[OI]/H α	HST-ID	Exposure s	P.A. °
NGC 2685*	S2/T2	S0 ₃ (7) pec	869	16.2	78	0.13b	8607	2585	54.4
NGC 2787	L1.9	SB(r)0+	691	13.0	63	0.55b	7361	1864	213.2
NGC 3368	L2	SAB(rs)ab	897	8.1	39	0.18	7361	1574	249.5
NGC 3489	T2	SAB(rs)0+	701	6.4	31	0.11b	7361	1644	239.1
NGC 3507	L2	SB(s)b	978	19.8	96	0.18	7357	900	89.9
NGC 3627*	T2/S2	S(s)bII.2	703	6.6	32	0.13	8607	2349	80.1
NGC 3675	T2	SA(s)b	766	1.8	9	0.12b	8607	2472	205.9
NGC 3953	T2	SB(r)bc	1053	17	82	0.12b	8607	2561	79.1
NGC 3992	T2:	SB(rs)bc	1048	17	82	0.13c	7361	1796	155.3
NGC 3998	L1.9	SA0	1049	21.6	105	0.53	8839	2827	304.3
NGC 4143	L1.9	SAB(s)0	783	17	82	0.71	7361	1707	139.0
NGC 4150*	T2	S0 ₃ (4)/a	244	9.7	47	0.13	8607	2395	240.1
NGC 4203	L1.9	SAB0-	1085	9.7	47	1.22b	7361	1630	105.6
NGC 4261	L2	E2+	2210	35.1	170	0.49	8236	1891	157.9
NGC 4314	L2	SB(rs)a	962	9.7	47	0.18b	7361	1668	105.3
NGC 4321	T2	SAB(s)bc	1234	16.8	81	0.11	7361	1642	92.9
NGC 4414	T2:	SA(rs)c	719	9.7	47	0.14u	8607	2395	125.1
NGC 4429	T2	SA(r)0+	1137	16.8	81	0.097u	8607	2349	81.1
NGC 4435	T2	SB(s)0	781	16.8	81	0.13b	7361	1644	89.6
NGC 4450	L1.9	SA(s)ab	1956	16.8	81	0.67	7361	1669	233.0
NGC 4459	T2	SA(r) 0+	1202	16.8	81	0.13u	7361	1644	92.9
NGC 4548	L2	SB(rs)b	485	16.8	81	0.23	7361	1644	73.2
NGC 4569*	T2	S0 ₃ (3)	-311	16.8	81	0.062	8607	2349	100.0
NGC 4596	L2::	SB(r)0+	1874	16.8	81	0.27u	7361	1671	250.3
NGC 4826*	T2	(R)SA(rs)ab	411	4.1	20	0.073	8607	2356	88.1
NGC 5055*	T2	S(s)bcII-III	516	7.2	35	0.17u	7361	1707	164.5
NGC 6503*	T2/S2	S(1)cII.8	26	6.1	30	0.08	8607	2687	315.1
NGC 7331*	T2	S(rs)bI-II	835	14.3	69	0.097u	8607	2395	358.9
NGC 278	H	SAB(rs)b	639	11.8	57	0.022b	7361	1786	47.6
NGC 3351	H	SB(r)b	778	8.1	39	0.019	7361	1671	245.6
NGC 4245	H	SB(r)0/a	890	9.7	47	0.038u	7361	1668	85.7
NGC 4800	H	SA(rs)b	808	15.2	74	0.041b	7361	1739	177.5
NGC 1023*	Abs	SB(rs)0	632	10.5	51	...	7566	2475	93.1

¹Galaxies labeled with * have been observed also at NOT.

Note. — Col. (1): Galaxy name; Cols. (2): Spectral class (according to HFS97 criteria); Cols. (3): Hubble type; Cols. (4): Radial velocity; Cols. (5): Distance; Cols. (6): Angular scale; Cols. (7): [OI]/H α flux ratio; Cols. (8): HST proposal ID number; Cols. (9): Exposure time; Cols. (10): Slit P.A.

3. Results

3.1. Central morphology and Nuclear spectral extractions

To extract the nuclear spectra of these galaxies, we have examined the spatial distribution of the continuum at 4700 Å along the slit. In all the objects, the central surface brightness is extended, with a symmetric distribution about the maximum, in many of them, this indicates that the bulge component dominates the central continuum light. LLAGN that have this type of distribution are: NGC 2787, NGC 3489, NGC 3992, NGC 4429, NGC 4450, NGC 4596, and NGC 7331. A few of the galaxies show a very sharp distribution that contains most of the central flux. These are NGC 3998, NGC 4321 and NGC 4569. While the sharp brightness distribution in NGC 4321 and NGC 4569 could be produced by a nuclear stellar cluster, the origin in NGC 3998 is not clear. Other objects, like NGC 3627, NGC 4150, NGC 4261, NGC 4435, NGC 4548, and NGC 6503, show a central complex structure, that could be produced by the superposition of dust lanes and several clusters randomly distributed or in a circumnuclear ring. To better inspect the central morphology of these LLAGN we have retrieved the WFPC2 optical images available in the HST archive. These images confirm the morphology suggested by the spectral central surface brightness profile. A detailed analysis of the central morphology and its relation with the nuclear stellar population is being carried out (González Delgado, in preparation). Figure 2 shows images and slit profiles of a few representative examples.

We have extracted two spectra for each galaxy (except in the case of NGC 4150, for which we have extracted three spectra, see Figure 3) corresponding to the central 0.3 arcsec (called *b* spectra) and 1 arcsec (called *a* spectra). These two extractions allow us to check if there is a change of the stellar population on a spatial scale of a few tens of parsecs. A direct comparison of the spectra of these two extractions indicates that the dominant stellar population on scales of 1 arcsec is also the dominant stellar population on the 0.3 arcsec scale.

Eight TOs (NGC 2685, NGC 3627, NGC 4150, NGC 4569, NGC 4826, NGC 5055, NGC 6503, NGC 7331) and NGC 1023 have also been observed by us from the ground. We have compared the *a* spectra with the nuclear spectra obtained from the ground. The strongest variations are found in NGC 4569 and NGC 4150, with a significant change in the shape of the continuum and/or the strength of the absorption lines. In the case of NGC 4569, the ground-based nuclear spectrum is somewhat redder and presents stronger metallic lines (such as the G band and CaII K) than the STIS *a* spectrum, indicating that a larger fraction of the bulge population contributes to the ground-based extraction (1×1.1 arcsec) compared to the STIS extraction (1×0.2 arcsec). In the case of NGC 4150 the differences in

the shape of the nuclear spectra can be associated with the dust lane structure that crosses the center and the different P.A. of the slit in the ground-based observation with respect to the STIS observations. In the remaining objects, the STIS and ground-based nuclear spectra are visually similar (see, e.g. NGC 3627 in Figure 4 on this paper and Figure 8 on Paper I), although some differences on the stellar populations are obtained through the empirical population analysis discussed in section 4.

3.2. Empirical stellar population classification

In Paper I LLAGN are classified empirically by comparing their spectra with those of non-active galaxies dominated by stellar population of different ages. The spectra were separated into four classes labeled by $\eta = Y, I, I/O$ and O :

- *Y*: Galaxies with young ($\leq 10^7$ yr) stellar population, characterized by a blue continuum and very diluted metallic absorption lines.
- *I*: Galaxies with a dominant intermediate age population (10^8 – 10^9 yr), characterized by prominent HOBLs in absorption.
- *I/O*: Galaxies with a mixture of intermediate age and older stars. These galaxies do not have visible HOBLs in absorption, but the metallic lines are weaker than in an old stellar population.
- *O*: Galaxies dominated by an old (10^{10} yr) stellar population, with strong metallic lines, such as CaK and H, CN, G band and MgII.

Here, we proceed in the same way comparing the STIS spectra with the template galaxies observed from the ground. Figures 4 to 7 group the weak and strong-[OI] LLAGN spectra in the I, I/O and O categories. As in Paper I, this classification is confirmed by modelling of the starlight by a combination of a base of five template galaxies representative of the O (NGC 1023 and NGC 2950), I/O (NGC 221), I (NGC 205) and Y (NGC 3367) classes. The results of this combination indicate that all the nuclei that belong to the O have relative contribution at 4020 Å of NGC 1023+NGC2950 larger than 75%, and those that belong to the I class have relative contribution at 4020 Å of NGC 205 larger than 30%. These results are in perfect agreement with the those obtained from the modelling of the stellar light using the population synthesis technique presented in section 4.

As in the ground-based spectra, none of the STIS LLAGN resembles pure young stellar systems. No features due to WR stars were detected directly in the STIS spectra of either

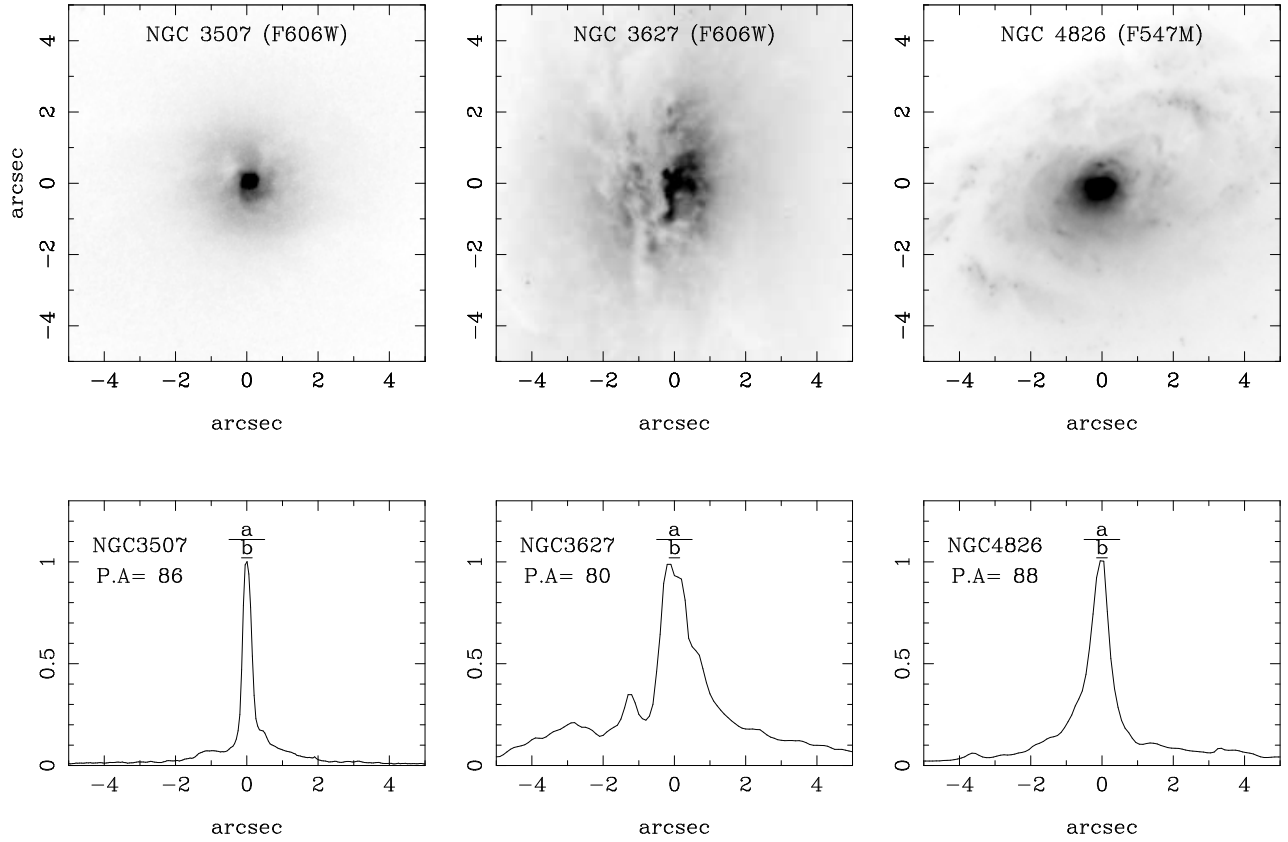


Fig. 2.— *Top*: WFPC2 images of NGC 3507, NGC 3627, and NGC 4826 through the filters F606W or F547M. North is up and East to the left. *Bottom*: Surface brightness profiles along the STIS slit of the optical continuum at 4700 Å. The extension of the *a* and *b* spectral extractions are marked by horizontal lines and labeled.

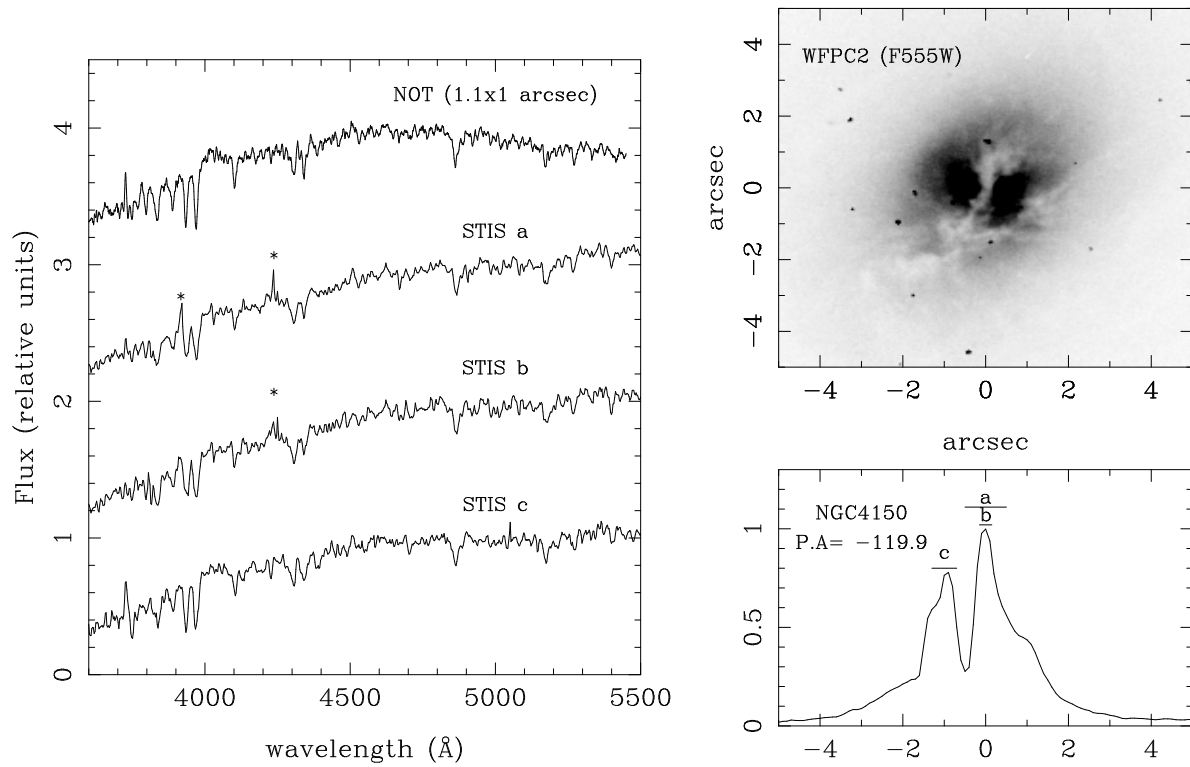


Fig. 3.— WFPC2 image through the F555W filter of NGC 4150, surface surface brightness profile along the STIS slit of the optical continuum at 4700 Å, and STIS spectra compared with the ground-based nuclear spectrum. The spectra are normalized to the flux at 4800 Å and shifted vertically for clarity.

LINERs or TOs, in neither extraction b (0.3×0.2 arcsec) nor a (1×0.2 arcsec). If WR stars are present in the nuclei of some LLAGN, they must contribute very little to the optical light, given that even observing through a very narrow slit, thus minimizing the bulge light, the broad bump at 4660 \AA is not detected. This result is also maintained when the spectra are subtracted of the intermediate and old stellar components (obtained through the template decomposition discussed above). Only in NGC 3507 we find a marginal evidence of a broad feature at 4620 \AA in the residual spectrum, although no broad feature at 4680 \AA is detected.

Most of the LLAGN spectra are dominated by starlight, with weak or absent nebular emission. Three LINERs (NGC 3998, NGC 4203, and NGC 4450), which are classified as L1.9 for presenting broad Balmer lines, are the exception (Figure 7b). These objects are among the strongest [OI]/H α emitters of the HFS97 sample, with values of 0.53, 1.22, and 0.67, respectively. Another important feature of these objects is that the stellar lines are very diluted with respect to the strength of these lines in a typical old and/or intermediate age population. This resembles what is observed in many Seyfert 2 galaxies (Schmitt et al 1999; González Delgado et al 2001; Cid Fernandes et al 2001a) in which the optical continuum is modelled by an old age population plus a feature less continuum (fitted by a power-law). In section 5 we discuss the origin of the continuum in these LINERs. None of the weak-[OI] LLAGN observed have such properties.

We find that an intermediate age population is more frequent in TOs (7/17) than in LINERs (2/11). Note, however, that both NGC 3368 and NGC 3507, the two $\eta = I$ LINERs, have [OI]/H α = 0.18, therefore trespassing the LINER/TO boundary of HFS97c by an insignificant amount. Expressed in terms of our weak and strong-[OI] classes (divided at [OI]/H α = 0.25), this difference becomes even more pronounced: 9/21 weak-[OI] but *none* of the strong-[OI] nuclei in the STIS sample present HOBLs. Taking these numbers together with the data from Paper I, we find that only 2 (NGC 841, [OI]/H α =0.58, and NGC 5005, [OI]/H α =0.65) out of the 24 (8%) strong-[OI] LLAGN belong to the $\eta = I$ class, while this fraction is 20/47 (42%) for weak-[OI]. As pointed out in Paper I, these numbers suggest a possible link between the central stellar population and emission line properties.

Figure 8 shows the STIS spectra of four HII nuclei (NGC 278, NGC 3351, NGC 4245, and NGC 4800) and one non-active galaxy (NGC 1023) to be compared with the LLAGN. Paradoxically, not all the HII nuclei show a continuum dominated by young and/or intermediate age population! In fact, the dominant central 0.3×0.2 arcsec stellar population in NGC 4245 and NGC 4800 is old ($\gtrsim 10^{10}$ yr) and somewhat similar to the non-active galaxy NGC 1023. However, the H α distribution in both objects is extended and more prominent in the off-nuclear spectra than in the central 0.3×0.2 arcsec, where H α is in absorption. It would be interesting to revise the emission line classification of these objects, and to check if

their HII denomination is associated to the large aperture of the spectra used in the HFS97 classification; then it is associated to star formation located in the circumnuclear region (100 pc to 1 kpc) than to the nucleus. This comparison also indicates the relevance of the central morphology of the continuum and emission lines in the classification of LLAGN.

3.3. Spectral properties

In this section we present measurements of spectral indices indicative of stellar populations for the STIS spectra. We list the measurements only for extractions a , since in most of the objects the differences in the spectral indices with respect to extractions b are small. We have measured 7 equivalent widths and two continuum colors in the system of Bica & Alloin (1986a,b): W_C , W_{wlb} , W_K , W_H , W_{CN} , W_G , W_{Mg} , F_{3660}/F_{4020} and F_{4510}/F_{4510} . These measurements were performed following the automated procedure devised in Paper I except for 3 cases (NGC 4459, NGC 4569 and NGC 6503), where the pseudo continuum was corrected by hand. We have also measured the 4000 Å break index ($D_n(4000)$), and the [OII] and H δ (H δ_A) equivalent widths following recipes in Balogh et al (1999) and Worthey & Ottaviani (1997).

Table 2 lists the results of these measurements. In Figure 9 we examine the relation between $D_n(4000)$, H δ_A and W_K for the combined STIS + ground samples. Different symbols correspond to stellar population classes $\eta = I, I/O$ and O (circles, triangles and squares respectively). Filled and open symbols are used for STIS and ground-based observations respectively. As discussed in Paper I, there is an excellent agreement between the empirical stellar population classes and the spectral indices. Nuclei with young and/or intermediate age populations ($\eta = I$) have low W_K and $D_n(4000)$, while for nuclei dominated by an old stellar population these indices assume large values, with $\eta = I/O$ objects in between.

4. Empirical Population Synthesis Analysis

4.1. The method

In order to quantify the stellar population mixture of LLAGN we use the empirical population synthesis (EPS) algorithm described in Cid Fernandes et al (2001b). Briefly, the code synthesizes a set of equivalent widths and colors by means of a combination of a base of 12 observed star clusters of different ages and metallicities (Schmidt et al 1991; Bica & Alloin 1986a,b) plus a $F_\nu \propto \nu^{-1.5}$ power-law to represent an AGN featureless continuum (FC). The output of the code consists of a *population vector* \vec{x} , whose components represent flux

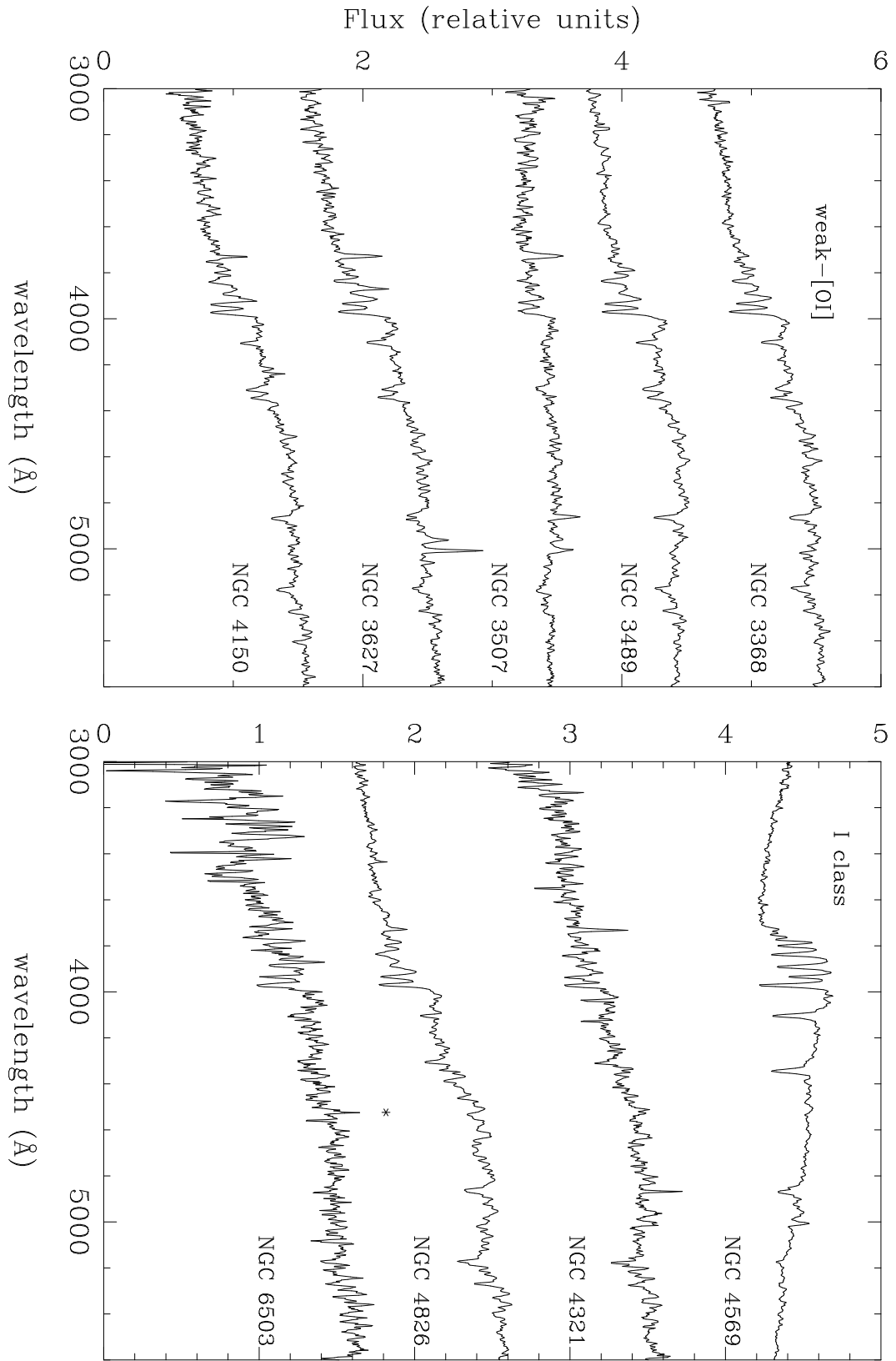


Fig. 4.— Nuclear spectra of weak-[OI] in the *I* class, i.e., with an intermediate age population.

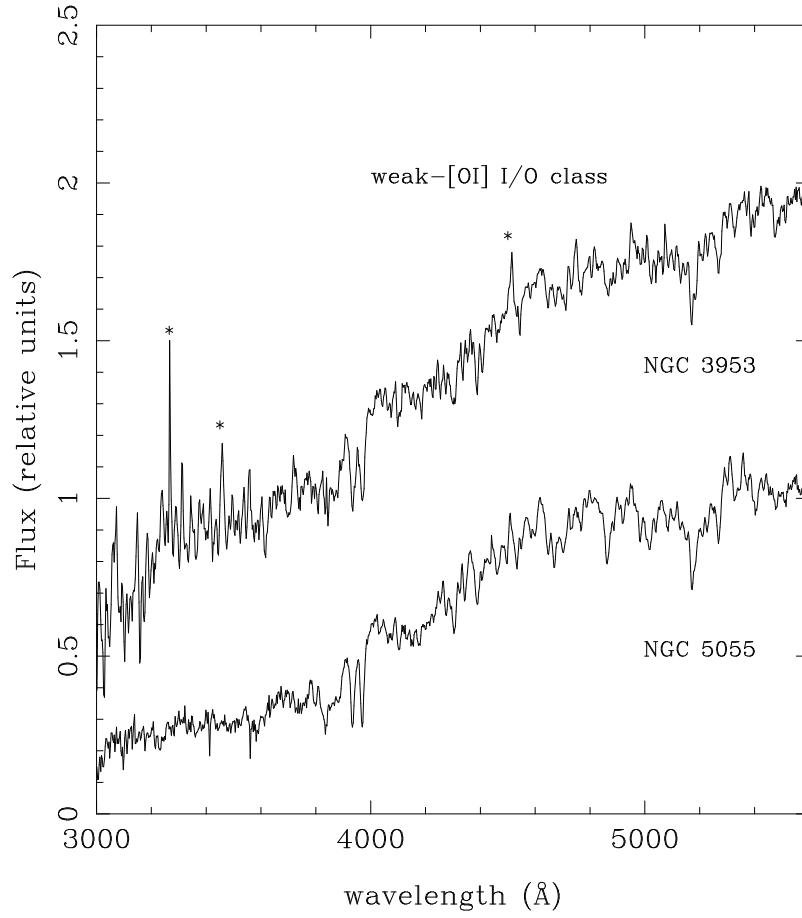


Fig. 5.— Nuclear spectra of weak-[OI] in the *I/O* class, i.e., with a mixture of intermediate age and older stars. Hot pixels in the spectra are labeled by *.

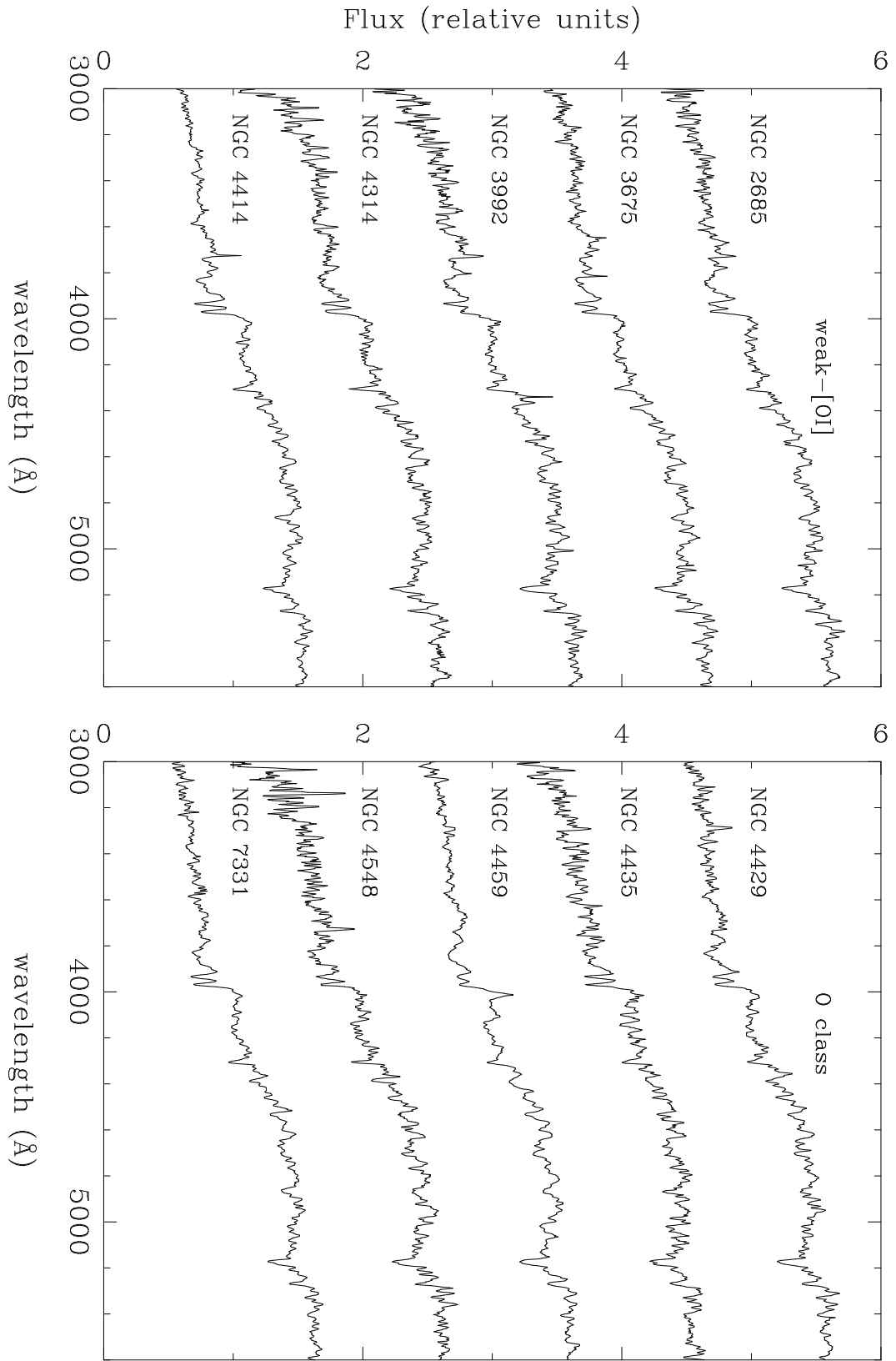


Fig. 6.— Nuclear spectra of weak-[OI] in the *O* class, i.e., with a predominantly old age population.

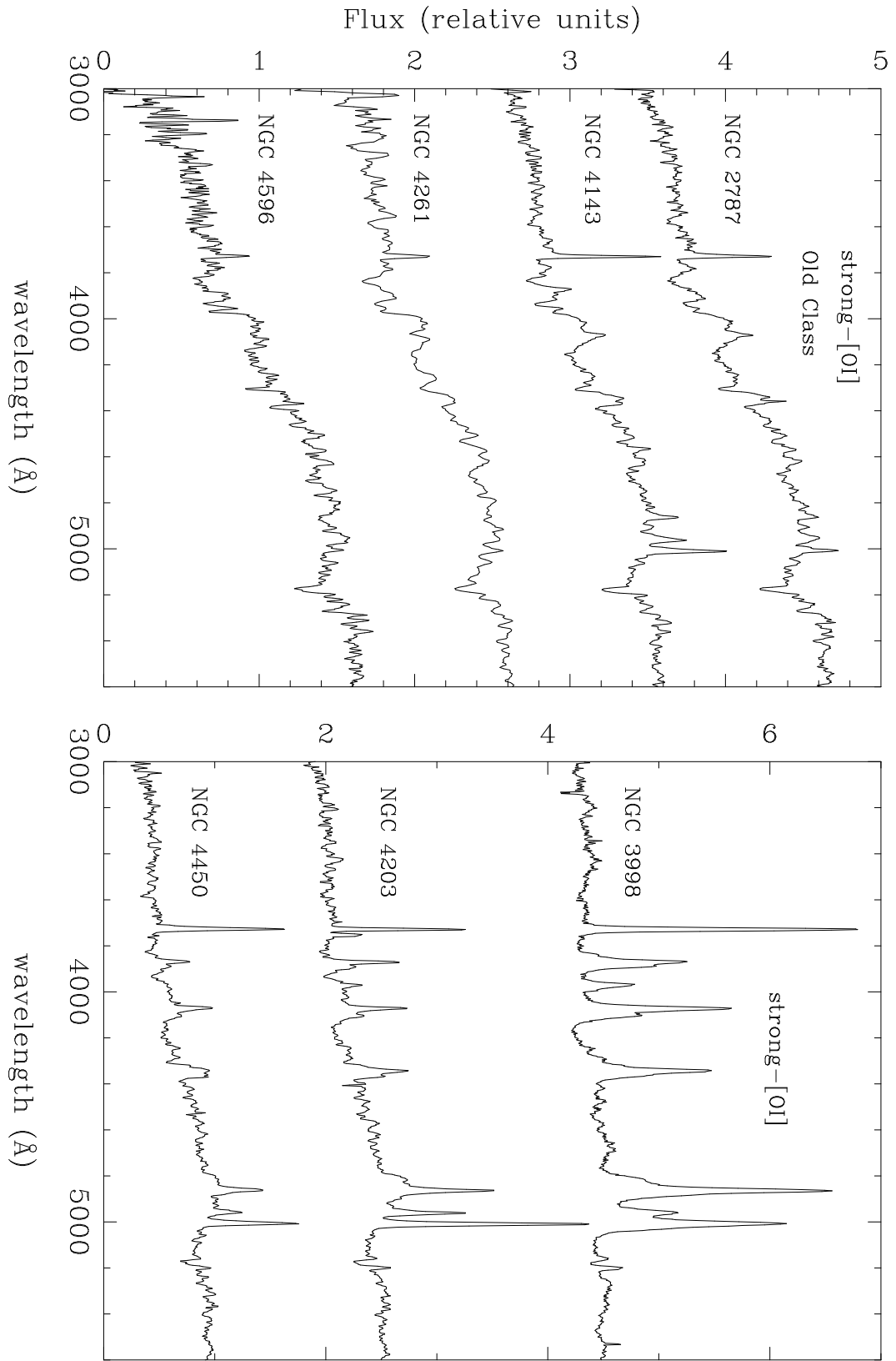


Fig. 7.— Nuclear spectra of strong-[OI]: (a) in the *O* class, i.e., with a predominantly old age population; (b) with diluted stellar lines

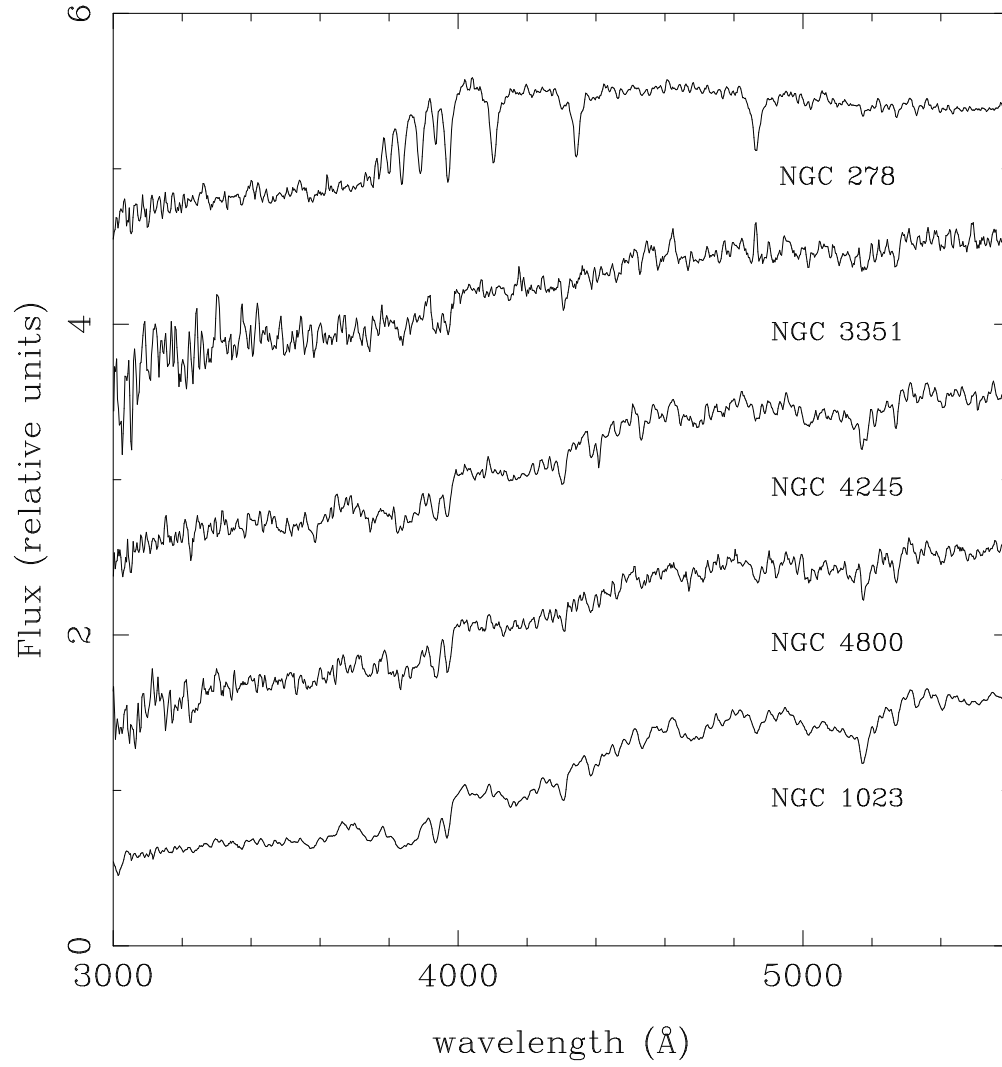


Fig. 8.— Nuclear spectra of a non-active galaxy, NGC 1023, and four HII nuclei.

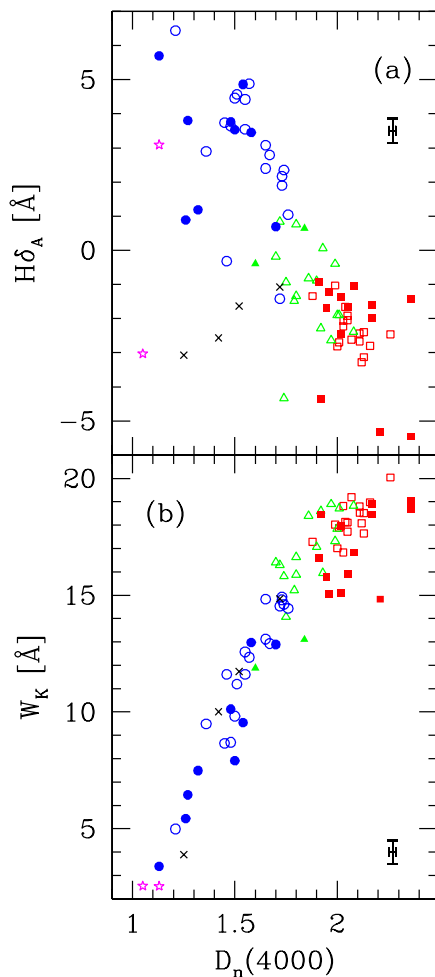


Fig. 9.— Relations between spectral indices: $D_n(4000)$, $H\delta_A$ and W_K . The stellar population classes I , I/O , O are represented by different symbols (circles, triangles and squares respectively). Except for the two stars, which represent the HII nuclei NGC 3367 and NGC 6217 from Paper I, only LLAGN are included. Crosses are used to represent NGC 3998, NGC 4143, NGC 4203 and NGC 4450, the four STIS sources with strong emission lines (Fig 7b). Filled and open symbols are used for STIS and ground-based observations respectively.

Table 2. Spectral properties in the *a* LLAGN STIS/CCD (G430L) spectra

Galaxy	W_C	W_{wlb}	W_K	W_H	W_{CN}	W_G	W_{Mg}	$\frac{F_{3660}}{F_{4020}}$	$\frac{F_{4510}}{F_{4020}}$	$D_n(4000)$	$H\delta_A$	$W(O\ II)$
NGC 2685	5.2	20.5	18.9	13.7	15.8	9.8	11.0	0.57	1.62	2.17	-1.6	2.1
NGC 2787	5.9	20.6	16.8	11.3	19.2	10.7	11.4	0.54	1.53	2.08	-1.0	26.1
NGC 3368	1.7	9.7	10.1	11.8	8.3	6.9	6.8	0.53	1.23	1.48	3.8	1.2
NGC 3489	2.2	12.2	13.0	12.3	8.8	7.9	7.4	0.56	1.16	1.58	3.5	-2.0
NGC 3507	1.0	4.1	5.4	6.6	4.6	4.6	4.9	0.81	1.03	1.26	0.9	6.5
NGC 3627	1.5	9.7	9.5	11.1	5.1	6.3	6.1	0.47	1.36	1.54	4.9	11.2
NGC 3675	2.3	18.6	18.4	13.2	16.3	10.4	10.9	0.60	1.71	2.17	-2.0	-2.4
NGC 3953	2.4	12.4	13.1	11.9	11.4	8.5	8.5	0.50	1.62	1.84	0.6	4.2
NGC 3992	3.3	19.0	18.7	12.7	17.6	10.5	11.1	0.46	1.67	2.36	-1.4	6.2
NGC 3998	1.2	-1.6	3.9	-6.1	12.7	0.3	4.8	0.93	1.25	1.25	-3.1	50.2
NGC 4143	3.4	14.2	14.8	8.2	17.4	8.7	11.5	0.63	1.49	1.72	-1.1	22.6
NGC 4150	2.0	9.5	7.9	10.4	5.5	7.4	5.8	0.54	1.38	1.50	3.5	5.5
NGC 4203	2.4	9.2	10.0	3.2	17.4	6.6	8.9	0.77	1.40	1.42	-2.6	19.2
NGC 4261	4.4	18.9	18.4	12.7	18.1	9.5	10.2	0.61	1.55	1.92	-4.4	12.0
NGC 4314	6.3	18.2	15.1	14.3	15.3	10.7	10.7	0.47	1.60	2.02	-2.5	-2.8
NGC 4321	-0.8	5.4	7.5	7.3	9.5	6.5	6.8	0.70	1.23	1.32	1.2	5.8
NGC 4414	3.6	16.5	16.6	12.7	14.7	9.8	9.4	0.55	1.42	1.91	-0.9	2.1
NGC 4429	4.9	19.8	15.8	13.4	18.5	10.4	12.2	0.52	1.60	1.95	-1.7	-1.8
NGC 4435	5.1	16.1	15.1	13.2	12.2	9.1	10.9	0.43	1.38	1.96	-1.2	-1.7
NGC 4450	3.7	11.0	11.7	6.4	14.5	7.9	9.0	0.74	1.42	1.52	-1.6	30.2
NGC 4459	4.5	18.3	14.8	11.4	15.5	10.1	11.9	0.62	1.78	2.21	-5.3	-2.3
NGC 4548	6.2	23.1	19.0	12.1	18.5	10.2	11.7	0.40	1.76	2.36	-5.4	10.5
NGC 4569	0.2	4.6	3.4	7.5	3.2	2.9	2.9	0.66	1.04	1.13	5.7	0.5
NGC 4596	4.0	17.0	15.9	11.6	15.9	9.7	11.0	0.55	1.56	2.05	-1.7	-1.0
NGC 4826	2.5	13.7	12.9	11.9	12.0	8.3	8.5	0.52	1.37	1.70	0.7	2.8
NGC 5055	3.0	12.9	11.9	10.3	13.9	7.1	10.9	0.63	1.48	1.60	-0.4	-1.7
NGC 6503	3.3	4.6	6.5	9.6	4.4	4.6	5.8	0.69	1.12	1.27	3.8	-1.5
NGC 7331	4.1	16.4	17.9	13.6	16.2	10.2	9.7	0.57	1.53	2.02	-1.4	-1.6
NGC 0278	0.2	7.8	4.3	12.2	3.9	4.3	3.5	0.39	0.90	1.31	10.1	-1.6
NGC 1023	5.7	21.5	19.3	14.0	21.6	11.6	12.6	0.57	1.61	2.32	-3.9	-4.3
NGC 3351	2.4	10.0	9.2	8.4	4.9	6.6	5.5	0.70	1.31	1.44	-0.5	-4.2
NGC 4245	3.8	16.4	14.4	11.0	16.7	11.0	11.1	0.58	1.67	1.93	-3.0	-2.8
NGC 4800	5.0	16.9	16.9	11.0	13.0	8.2	8.5	0.62	1.55	1.93	-2.1	-2.9

Note. — Col. (1): Galaxy name; Cols. (2–10): Equivalent widths of seven absorption features and two colors, all in Bica & Alloin system. Col. (11): 4000 Å break index (Balogh et al 1999). Col. (12): $H\delta_A$ equivalent width of Worthey & Ottaviani (1997). Col. (13): [OII] equivalent width of Balogh et al (1999).

fractions associated with each population in the base, plus the V-band extinction, modelled as due to a uniform dust screen. These parameters correspond to a likelihood-weighted mean of 10^8 combinations obtained from a Metropolis tour through the (\vec{x}, A_V) space. We use as input to the EPS code five spectral indices: W_K , W_{CN} , W_G plus the F_{3660}/F_{4020} and F_{4510}/F_{4020} colors. This same set of observables was used in the EPS analysis of Starburst (Cid Fernandes, Leão & Rodrigues Lacerda 2003b) and Seyfert 2 galaxies (Cid Fernandes et al. 2001a), which provide an important reference for comparison.

The virtues and shortcomings of EPS have been extensively discussed in Cid Fernandes et al. (2001b, 2003b). Our experience with this method in a variety studies has taught us that it is a superb tool to analyse stellar population mixtures provided that one keeps the description at a relatively coarse level. Accordingly, in this paper we group components of same age in a reduced population vector $\vec{x} = (x_{FC}, x_6, x_7, x_8, x_9, x_{10})$ where x_6 – x_{10} correspond to five logarithmically spaced ages of 10^6 , 10^7 , 10^8 , 10^9 and 10^{10} yr, and x_{FC} corresponds to the power-law component. Even this description is too fine graded given the limitations of the EPS imposed by the combination of observational errors, limited input information and quasi-linear dependences within the base. We therefore base our analysis of the EPS results on an even coarser (but more robust) description obtained by further grouping similar \vec{x} components. For instance, although the method does not distinguish well between the 10^6 , 10^7 and FC individual components, their sum $x_{Y/FC} \equiv x_{FC} + x_6 + x_7$ is well constrained. Similar rebinnings of the remaining components are employed in the discussion below.

We have also calculated formal errors and covariances for three condensed EPS fractions ($x_{Y/FC}$, x_8 and x_{9+10}). The average errors are 2.2%, 3.2%, and 3.2%, respectively. These errors are low, and allow us to distinguish between the different components with a precision of about 3%. However, this does not apply for old systems with a contribution of $x_{9+10} \geq 90\%$. In these objects, the fractions $x_{Y/FC}$ and x_8 obtained are similar to the formal errors, and in consequence these values are not significant.

4.2. Statistical results

Tables 3 and 4 list the EPS results for both the ground-based and STIS samples. The population vector is expressed as the percentage fraction of the flux at a normalization wavelength of 4020 Å. In this section we present histograms of the results of the synthesis grouped in three age bins, used to represent old (10^{10} yr, x_{10}), intermediate populations (10^8 – 10^9 yr, $x_8 + x_9$) and young plus FC components ($x_{Y/FC}$). In these histograms we divide the LLAGN in weak-[OI] ($[OI]/H\alpha \leq 0.25$) and strong-[OI] ($[OI]/H\alpha \geq 0.25$) sources.

Figure 10 shows the results for the ground-based observations only. The average (median) values of the distributions of the old, intermediate and young stellar population of the weak-[OI] LLAGN are: 48% (47%), 46% (45%) and 6% (5%), respectively. For the strong-[OI] LLAGN these values are: 62% (64%), 35 % (33%) and 3% (3%). A remarkable result from this analysis is that the Y/FC component rarely exceeds 10% of the flux in the 1.1×1 arcsec ground-based aperture. This only happens in 5/51 (10%) of our LLAGN (NGC 772, NGC 4569, NGC 5377, NGC 5678 and NGC 6503), all of which are weak-[OI] sources. Another significant difference between strong and weak-[OI] is found in the fraction of intermediate age population. The fraction of weak-[OI] LLAGN with $x_I = x_8 + x_9 > 35\%$ is 25/34 (74%), but only 5/17 (29%) for strong-[OI]. Regarding the old stellar population, the fraction of weak-[OI] nuclei with $x_{10} < 65\%$ is 27/34 (79%) and 10/17 (59%) for strong-[OI]. These numbers essentially translate the analysis done in Paper I to population strengths, and clearly indicate that weak-[OI] LLAGN are nuclei with an important intermediate age population.

Figure 11 shows the results for the STIS a spectra. The EPS analysis has also been done for the b spectra, but we have not found a significant difference between the results for the two apertures. The previous conclusion that weak-[OI] LLAGN have a larger contribution from the intermediate age population than strong-[OI] LLAGN is still valid. In 16 of the 21 (76%) weak-[OI] but only 2/7 (28%) of the strong-[OI] LLAGN the contribution of the intermediate age population is larger than 35%. However, there is a noticeable difference with respect to the ground-based observations, related with the strength of young plus FC component. The mean value of this component is $x_{Y/FC} = 12\%$ and 22% for weak and strong-[OI] LLAGN respectively. These values are larger than the mean contributions in the ground-based spectra, 3% and 6%, respectively. There are four weak-[OI] (NGC 3507, NGC 4321, NGC 4569, and NGC 6503) and three strong-[OI] LLAGN (NGC 3998, NGC 4203, and NGC 4450) with $x_{Y/FC} > 20\%$, whereas only NGC 4569 has such a strong component in the ground based data. These three LINERs show very strong emission lines and diluted stellar lines, probably produced by the contribution from an AGN component (see section 5.1). On the other hand, in NGC 3507, NGC 4321, NGC 4569 and NGC 6503, the UV emission and the spectral characteristics of the optical spectra suggest that the large contribution from the Y/FC component is provided by a young stellar cluster. This cluster must be compact, as indicated by the morphology in the WFPC2 images and surface brightness profile along the slit, and hence its contribution to the optical light is much less important into a ground-based aperture. It is interesting to note that in the ground-based aperture, NGC 4569 and NGC 6503 outstand for their large intermediate age population.

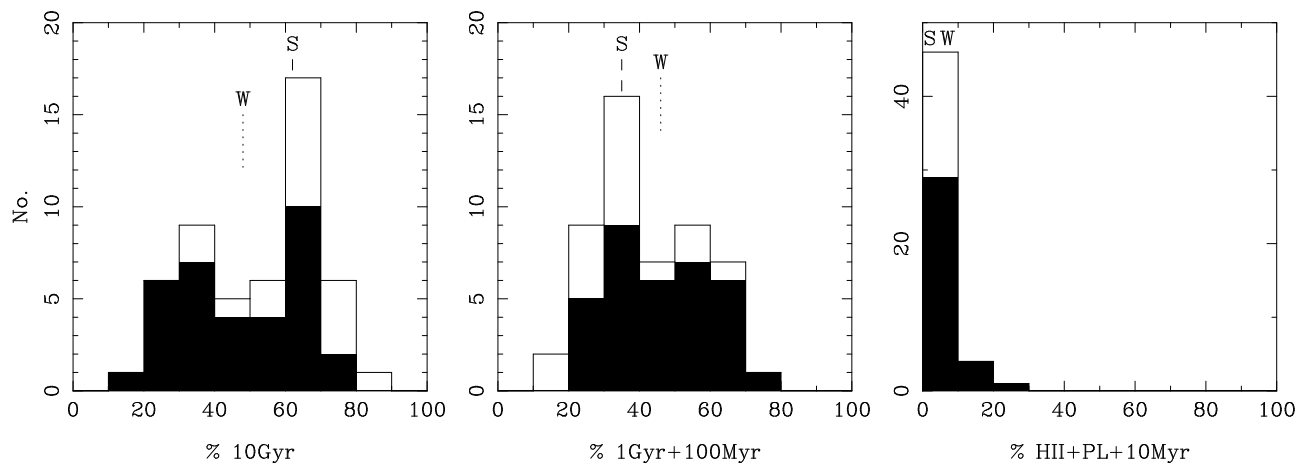


Fig. 10.— Histograms of the contribution of different age components, normalized to the light at 4020 \AA . The histogram is for the ground-based observations, thus corresponding to stellar populations that contribute to a nuclear aperture of 1.1×1 arcsec. The filled area represents the distributions of weak-[OI] LLAGN. Labels W and S indicate the median corresponding to the distributions of weak and strong-[OI] LLAGN respectively.

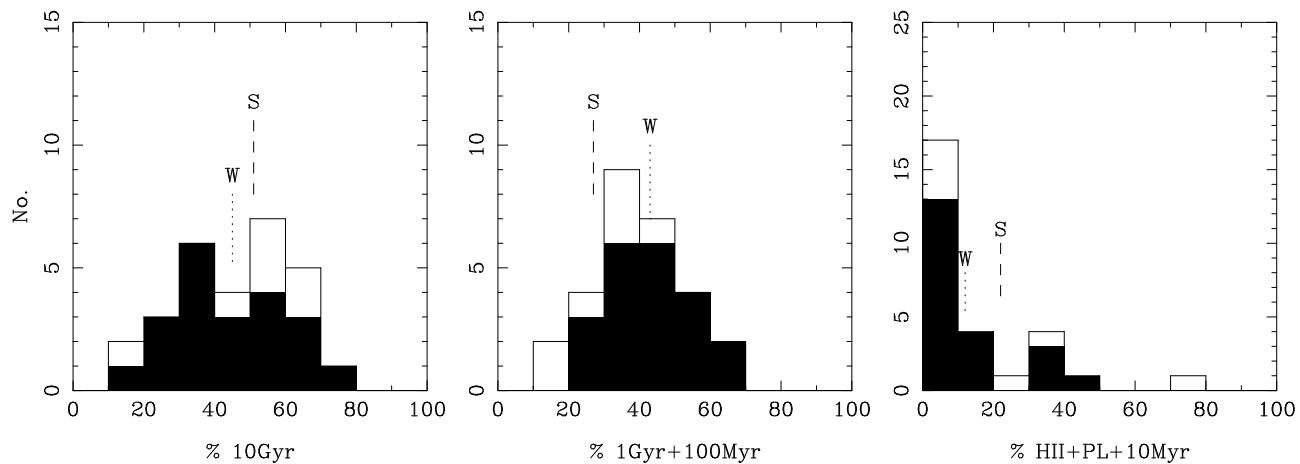


Fig. 11.— As Figure 10 but for STIS *a* spectra (corresponding to the nuclear 1×0.2 arcsec).

Table 3. EPS results for the ground-based observations

Galaxy	x_{10}	x_9	x_8	x_7	x_6	x_{PL}	A_V
NGC 0266	63.3	33.0	1.8	1.0	0.4	0.4	0.28
NGC 0315	68.2	23.3	3.6	2.6	1.2	1.1	0.34
NGC 0404	27.3	35.7	28.7	4.4	1.9	1.9	1.56
NGC 0410	65.6	27.7	3.1	1.9	0.8	0.8	0.30
NGC 0428	25.6	64.4	6.3	2.1	0.8	0.9	0.79
NGC 0521	61.4	33.4	2.7	1.3	0.6	0.6	0.56
NGC 0660	42.0	48.4	5.1	2.5	1.0	1.1	2.37
NGC 0718	36.3	46.1	11.6	3.3	1.4	1.4	0.74
NGC 0772	46.9	24.4	11.5	8.7	4.9	3.5	0.28
NGC 0841	39.5	49.9	6.1	2.5	1.0	1.1	0.57
NGC 1052	70.1	20.8	3.9	2.8	1.2	1.1	0.37
NGC 1161	75.5	20.9	1.8	1.0	0.4	0.4	0.24
NGC 1169	73.2	22.9	1.7	1.2	0.5	0.5	0.15
NGC 2681	25.7	52.7	16.1	3.0	1.2	1.3	0.91
NGC 2685	65.2	31.3	1.8	1.0	0.4	0.4	0.26
NGC 2911	64.4	29.7	3.1	1.5	0.7	0.6	0.80
NGC 3166	42.9	48.3	4.9	2.1	0.9	0.9	0.62
NGC 3169	50.2	44.2	3.0	1.5	0.6	0.6	1.15
NGC 3226	78.3	16.4	2.4	1.5	0.7	0.6	0.53
NGC 3245	59.4	27.4	5.2	4.2	2.0	1.8	0.33
NGC 3627	29.6	47.1	16.7	3.6	1.4	1.5	1.14
NGC 3705	36.7	52.6	6.5	2.3	0.9	1.0	1.08
NGC 4150	29.2	52.3	12.7	3.2	1.2	1.3	0.62
NGC 4192	52.6	38.1	4.5	2.6	1.1	1.1	1.77
NGC 4438	67.2	27.2	2.8	1.5	0.7	0.6	1.15
NGC 4569	19.6	13.2	45.7	11.0	5.0	5.4	0.35
NGC 4736	36.8	43.9	12.6	3.7	1.6	1.5	0.68
NGC 4826	44.6	40.1	9.6	3.1	1.3	1.3	0.67
NGC 5005	34.4	53.4	7.4	2.6	1.0	1.1	1.38
NGC 5055	46.1	34.1	12.4	4.0	1.7	1.7	0.81
NGC 5377	31.1	24.3	32.5	6.2	3.1	2.8	0.64
NGC 5678	34.8	31.8	22.1	5.9	2.7	2.8	1.85
NGC 5879	33.7	60.5	3.3	1.4	0.5	0.6	0.89
NGC 5921	29.8	45.2	17.6	4.1	1.6	1.8	0.68
NGC 5970	60.7	35.8	1.6	1.0	0.4	0.5	0.18
NGC 5982	58.7	36.7	2.2	1.3	0.5	0.5	0.21
NGC 5985	65.0	31.4	1.7	1.0	0.4	0.5	0.22
NGC 6340	85.4	12.0	1.3	0.7	0.3	0.3	0.91
NGC 6384	69.1	27.4	1.4	1.1	0.5	0.5	0.13
NGC 6482	69.7	26.4	1.7	1.2	0.5	0.5	0.13
NGC 6500	60.8	26.4	3.6	4.9	2.4	1.8	0.12
NGC 6501	63.1	28.3	4.4	2.2	1.0	0.9	0.42
NGC 6503	39.3	31.4	12.6	8.7	3.9	4.1	0.43
NGC 6702	62.8	32.4	2.1	1.4	0.6	0.6	0.21
NGC 6703	71.3	24.3	2.1	1.2	0.5	0.5	0.31
NGC 6951	51.2	40.8	4.5	1.9	0.8	0.8	0.37
NGC 7177	60.5	32.4	3.4	2.0	0.9	0.9	0.57
NGC 7217	75.7	20.8	1.7	0.9	0.4	0.4	0.41
NGC 7331	61.8	33.3	2.5	1.3	0.6	0.6	0.43
NGC 7626	69.4	25.1	2.6	1.6	0.7	0.6	0.27
NGC 7742	52.3	41.6	3.2	1.5	0.6	0.7	0.64
NGC 3367	9.1	6.4	5.3	31.9	32.5	14.8	0.11
NGC 6217	11.2	6.7	34.2	16.5	17.4	13.9	0.26
NGC 0205	25.4	24.5	38.5	5.9	2.8	2.8	0.60
NGC 0221	56.4	39.1	2.1	1.3	0.6	0.6	0.20
NGC 0224	67.1	25.5	3.2	2.3	1.0	0.9	0.22
NGC 0628	55.8	37.4	2.9	2.0	0.8	0.9	0.35
NGC 1023	79.6	17.3	1.5	0.9	0.4	0.4	0.16
NGC 2950	60.0	33.4	3.1	1.9	0.8	0.8	0.23
NGC 6654	75.2	20.6	1.9	1.3	0.6	0.5	0.14

Table 4. EPS results for the STIS a data

Galaxy	x_{10}	x_9	x_8	x_7	x_6	x_{PL}	A_V
NGC 2685	66.4	29.4	2.0	1.2	0.5	0.5	0.51
NGC 2787	60.5	31.4	4.4	2.1	0.9	0.8	0.38
NGC 3368	33.1	31.7	24.8	5.5	2.5	2.4	0.73
NGC 3489	32.1	50.5	10.9	3.5	1.4	1.5	0.31
NGC 3507	26.8	14.4	14.7	17.4	15.2	11.5	0.25
NGC 3627	31.7	36.5	22.3	5.1	2.2	2.2	1.66
NGC 3675	74.1	20.3	2.5	1.7	0.7	0.7	0.59
NGC 3953	42.5	36.5	12.8	4.4	1.9	1.9	1.72
NGC 3992	59.1	37.4	1.9	0.9	0.4	0.4	0.91
NGC 3998	15.5	5.8	5.7	33.7	20.7	18.6	1.47
NGC 4143	57.0	24.7	8.5	5.3	2.4	2.1	0.43
NGC 4150	39.3	20.6	22.0	7.9	5.7	4.5	1.48
NGC 4203	48.9	8.6	9.0	15.3	11.9	6.3	0.51
NGC 4261	65.4	29.2	2.5	1.6	0.6	0.7	0.25
NGC 4314	51.7	34.8	8.6	2.6	1.2	1.1	1.10
NGC 4321	35.5	12.9	19.0	13.3	11.5	7.7	0.56
NGC 4414	48.0	44.0	4.2	2.0	0.8	0.8	0.44
NGC 4429	59.4	28.0	7.6	2.7	1.2	1.1	0.72
NGC 4435	27.8	61.6	7.1	1.9	0.8	0.8	1.17
NGC 4450	53.4	13.6	8.4	12.1	7.6	5.0	0.41
NGC 4459	65.4	17.2	6.3	5.6	3.1	2.3	1.25
NGC 4548	57.9	39.1	1.6	0.7	0.3	0.3	1.26
NGC 4569	14.6	9.1	40.9	13.2	11.1	11.0	0.79
NGC 4596	54.0	34.3	6.4	2.9	1.2	1.2	0.79
NGC 4826	39.6	37.0	15.9	4.1	1.7	1.7	0.82
NGC 5055	44.0	24.0	14.1	9.5	4.5	3.9	1.08
NGC 6503	28.7	19.3	21.4	14.3	8.1	8.2	0.72
NGC 7331	60.4	34.1	2.7	1.5	0.6	0.6	0.39
NGC 0278	11.8	10.1	71.1	3.4	1.8	1.8	0.40
NGC 1023	78.7	18.3	1.3	0.9	0.4	0.3	0.12
NGC 3351	45.3	22.6	9.3	10.7	6.5	5.7	0.95
NGC 4245	64.8	16.3	9.0	5.0	2.9	2.0	0.89
NGC 4800	55.4	36.4	3.6	2.5	1.0	1.1	0.81

5. Discussion

5.1. Comparison with non-active galaxies

The EPS analysis suggests that many of the LLAGN have a 10^8 – 10^9 yr intermediate age stellar population which is far more conspicuous in weak-[OI] than in strong-[OI] nuclei. The question arises whether these statistics are the typical stellar population of early type galaxies, or intermediate age stars are more significant in LLAGN than in non-active galaxies of the same morphological type.

Raimann et al (2003) have analyzed the stellar population of a small sample of S0 to Sbc non-active galaxies using the same EPS code and star cluster base. They find that the old and the intermediate age population contributes with $x_O = 65\%$ and $x_I = 35\%$ to the continuum at 4020 \AA . The mean contributions in our ground-based aperture are $x_O = 62\%$ and $x_I = 35\%$ for strong-[OI] and $x_O = 48\%$ and $x_I = 46\%$ for weak-[OI] LLAGN. On the other hand, the intermediate age population contributes with $x_I \geq 35\%$ in 74% of the weak-LLAGN, while this happens in only 29% of the strong-[OI]. These results suggest that weak-[OI] LLAGN have an intermediate age population that is more significant than in non-active galaxies, and have less contribution of the old population than in non-active galaxies.

5.2. Emission line versus stellar population

In Paper I we found a strong tendency of the HOBLs to appear preferentially in weak-[OI] LLAGN. As discussed in §3.2, this result also applies to the STIS observations. The detection of these lines implies the presence of a substantial intermediate age population (e.g. González Delgado et al 1999). This suggestion is confirmed by the EPS analysis done here, which shows that LLAGN with conspicuous HOBLs (i.e. those classified $\eta = I$) have $x_8 + x_9 \geq 30\%$. The statistical connection between these populations and the weak-[OI] class is clearly illustrated in Figures 10–11, which show that weak-[OI] LLAGN have systematically higher contribution of intermediate age populations. These results suggest a connection between LLAGN subtypes and their stellar population. Because these two classes differ in their emission line properties, this connection implies a link between the stellar population and the ionization process in LLAGN.

In Paper I, we have noted a dichotomy between the [OI]/H α ratio and the spectral indexes, that indicates that there are no strong-[OI] LLAGN with conspicuous HOBLs and with $W_K \leq 15 \text{ \AA}$ and $W_C \leq 3.5 \text{ \AA}$. These results are also confirmed by the EPS analysis, and are shown in Figure 12 where we plot [OI]/H α as a function of the fraction of the

light provided by the old and the intermediate age stellar populations. The $[\text{OI}]/\text{H}\alpha$ vs. x_O diagram has an 'inverted L' shape, that can be interpreted as the strong- $[\text{OI}]$ LLAGN having a stellar population mainly dominated by old stars, while weak- $[\text{OI}]$ LLAGN can have stellar populations of all ages. However, the $[\text{OI}]/\text{H}\alpha$ vs. x_I diagram is 'L' shaped, showing that many of the weak- $[\text{OI}]$ LLAGN have higher x_I . This also confirms that most of the objects with intermediate age are weak in $[\text{OI}]$. As we suggested in Paper I, in these objects stellar sources can dominate the ionization, and we call them stellar-LLAGN.

We use the STIS spectra to look for these sources. The high spatial resolution provided by STIS is crucial to detect compact young stellar clusters, that otherwise can be masked by the underlying light emitted by the old stars in ground based observations. The EPS analysis finds that only 5 weak- $[\text{OI}]$ of the 34 observed from the ground have a young component with $x_{Y/FC} \geq 10\%$. These objects belong to the *I* class; and have $x_I \geq 30\%$. However, the STIS EPS analysis finds a larger fraction of weak- $[\text{OI}]$ LLAGN with a young stellar component, in particular among those that belong to the *I* class. In fact, 7 of the 9 weak- $[\text{OI}]$ LLAGN in the *I* class have $x_{Y/FC} \geq 10\%$. In addition, two more weak- $[\text{OI}]$ LLAGN, NGC 5055 and NGC 4459, that belong to the *I/O* and *O* class respectively, have $x_{Y/FC} \geq 10\%$. All of these objects have an important contribution of the intermediate age stars. It is also important to note that in several objects in which the young stellar population was not detected in the ground-based observations, it has been detected in the STIS spectra. This suggests that some weak- $[\text{OI}]$ LLAGN that are classified as *I/O* can have a very compact young cluster that is detected when observed with a small aperture, as it is the case of NGC 5055.

Further evidence that these objects have young stellar clusters come from the UV observations reported by Maoz et al (1998). They found UV resonance lines formed in the wind of massive stars in NGC 404, NGC 4569, and NGC 5055, and possibly in NGC 6500. NGC 3507 also shows similar UV features (González Delgado et al. in preparation). All these are weak- $[\text{OI}]$ LLAGN and outstand at optical wavelengths for their intermediate age population. Note, however, that only NGC 4569 has $x_{Y/FC} \geq 10\%$ in the ground-based aperture. We can thus conclude that weak- $[\text{OI}]$ LLAGN that belong to the *I* or *I/O* class, and therefore have an important intermediate age population, are stellar-LLAGN.

In the strong- $[\text{OI}]$ LLAGN, stars cannot play an important role in the gas ionization because we have not found a noticeable presence of stars younger than 1 Gyr. Photoionization by an AGN is likely the dominant emission line mechanism in these sources. NGC 5005 could be the exception to this, because it is a strong- $[\text{OI}]$ LLAGN with HOBLs, and so has an intermediate age. An AGN as the dominant source of ionization in LLAGN can clearly be represented by the strong- $[\text{OI}]$ NGC 3998, NGC 4203, and NGC 4450, for which we have obtained $x_O \leq 50\%$, and $x_{Y/FC} \geq 20\%$.

As pointed out by Cid Fernandes & Terlevich (1995), a young stellar population has an optical continuum very similar in shape to a power-law. There is thus a degeneracy between the young stellar and the power-law components in the EPS analysis. This degeneracy can be broken only at ultraviolet wavelengths. If the resonance lines of CIV $\lambda 1550$, SiIV $\lambda 1400$, NV $\lambda 1240$ formed in the wind of massive stars are detected, then the optical light is provided by a young starburst. We have retrieved from the HST archive the UV spectrum of NGC 3998 to search for wind lines, but they are not present in the spectrum. On the contrary, broad CIV and $L\alpha$ emission lines are detected. Furthermore, the optical spectrum shows also many FeII multiplets, and the Balmer lines have a broad component. These spectral features suggest that a Seyfert 1 nucleus dwells in this strong-[OI] LLAGN. NGC 4203 and NGC 4450 have not been observed at the UV with the HST, so we can not check for the presence of wind stellar lines. However, their optical spectra show double-peaked broad H lines (Ho et al 2000; Shields et al 2000). This detection is interpreted as the presence of a nuclear accretion disk in these two galaxies. We thus conclude that the high $x_{Y/FC}$ component derived from the EPS analysis of these two galaxies is due to a non-thermal optical continuum that can be represented by a power-law. Therefore, NGC 3998, NGC 4203 and NGC 4450 are strong-[OI] LLAGN that harbor a dwarf-Seyfert 1 nucleus; they are probably AGN-LINERs. Note, however, that none of these three galaxies outstands in the 'inverted L' of Figure 2 in Paper I. As expected, weak AGN can easily be masked by the contribution of the stellar population in a typical ground-based aperture observation. So it could be that other strong-[OI] have less luminous AGNs than those in NGC 3998, NGC 4203 and NGC 4450 contributing to the optical continuum with less than 10% of the 4020 Å light in a 0.2×1 arcsec aperture. NGC 2787 and NGC 4143 are two possible cases because they have a broad $H\alpha$ emission component and have been classified by Ho et al (1997a) as L1.9, but with a less luminous AGN because $x_{Y/FC} \leq 10\%$.

5.3. Mean age of the stellar population

In Figure 13 we condense the results of the EPS analysis in the evolutionary diagram devised by Cid Fernandes et al. (2003b). The trick consists of grouping the population vector onto just 3 components, which, because of normalization, are confined to a plane in this 3D space, such that all components may be visualized in a 2D projection. We choose to group the 10^6 , 10^7 yr and power-law components in a $x_{Y/FC}$ component (as we did in the statistical discussion above) and plot it against the 10^8 yr fraction (x_8). The two remaining components, x_9 and x_{10} , run along a third, perpendicular axis. The dotted lines in Figure 13 indicate lines of constant $x_{9+10} \equiv x_9 + x_{10}$, as labeled. With these choices, young systems are located in the bottom right of this diagram, while $\sim 10^8$ yr populations appear in the top left and systems

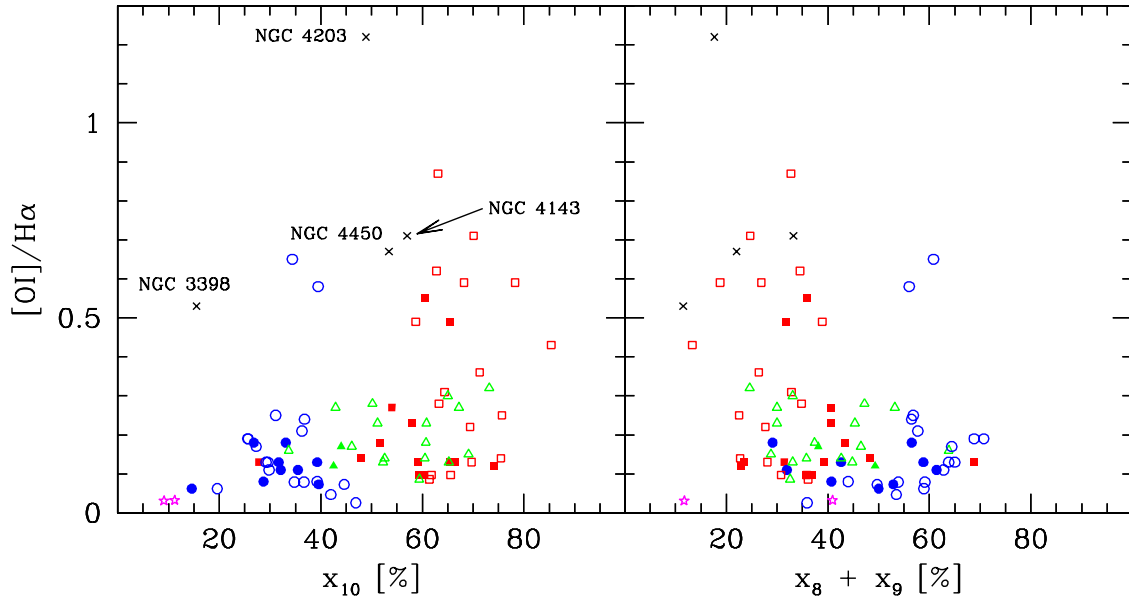


Fig. 12.— $[OI]/H\alpha$ vs fraction of the light provides by: (a) old (10Gyr), and (b) intermediate (1Gyr+100Myr) age population. Symbols are as in Figure 9.

dominated by populations of 10^9 yr or more occupy the bottom left corner. In other words, evolution proceeds counter-clockwise in this handy diagnostic diagram of stellar populations (see Cid Fernandes et al 2003b for details).

A first result which strikes the eye in this plot is the neat correspondence between the EPS results and the empirical stellar population classification. All but one of the $\eta = \text{I}$ objects are located above the $x_{9+10} = 90\%$ line, whereas most of the $\eta = \text{O}$ sources fall below this limit, with $\eta = \text{I/O}$ objects roughly in between. This correspondence, previously discussed in our statistical considerations (§4.1), is simply the EPS version of the excellent relationship between η and the input spectral indices.

The distribution of LLAGN in Figure 13 is suggestive of an evolutionary sequence, similar to that outlined in Paper I to explain the $[\text{OI}]/\text{H}\alpha$ versus W_K diagram. In order to investigate evolutionary effects in more detail we have carried out an EPS analysis of theoretical galaxy spectra computed with the GISSEL96 evolutionary synthesis code of Bruzual & Charlot (1993), processed through our EPS machinery in exactly the same manner as for the LLAGN data. Details of this “calibration” of EPS results in terms of evolutionary synthesis models are described in Cid Fernandes et al (2003b), where, except for the inclusion of a power-law in the base, these same calculations were first discussed. Models were computed for a pure instantaneous burst (IB) with ages from 0 to 15 Gyr and for mixtures of an evolving IB and a fixed 15 Gyr population. These mixed models are parametrized by the contrast parameter c_0 , the fraction of the 4020 Å flux which is associated with the 15 Gyr old population when the burst starts ($t = 0$). These simplistic scenarios for the star-formation history provide a useful reference for a qualitative evaluation of evolutionary effects.

In Figure 14a we overlay these models with the LLAGN data in our evolutionary diagram. The outer solid line traces the evolution of a pure IB. The ages (in Myr) of some of the 21 models computed are indicated. Other solid lines in this plot correspond to mixed models with contrast parameters $c_0 = 40, 60$ and 80% (from left to right, respectively). Notice that the evolutionary path of mixed models is similar in shape to that of a pure IB, but with much reduced amplitudes of the 10^8 yr and younger components. After ~ 0.5 Gyr all models merge in the sequence towards large x_{9+10} in the bottom left of the plot.

The location of the LLAGN in the above diagram reinforce our hypothesis that LLAGN line up in what looks to be an evolutionary sequence, from $\eta = \text{I}$ to O . Similar conclusion can be reached comparing the location of these sources in the $D_n(4000)$ versus $H\delta_A$ diagram with those of the models of Kauffmann et al (2003). The transition from $\eta = \text{I}$ to O occurs at 1–2 Gyr, depending on c_0 . From the discussion in §5.1, this is also an evolutionary sequence in emission line properties, from $\eta = \text{I}$ and weak-[OI] to $\eta = \text{O}$ and either weak or strong-[OI].

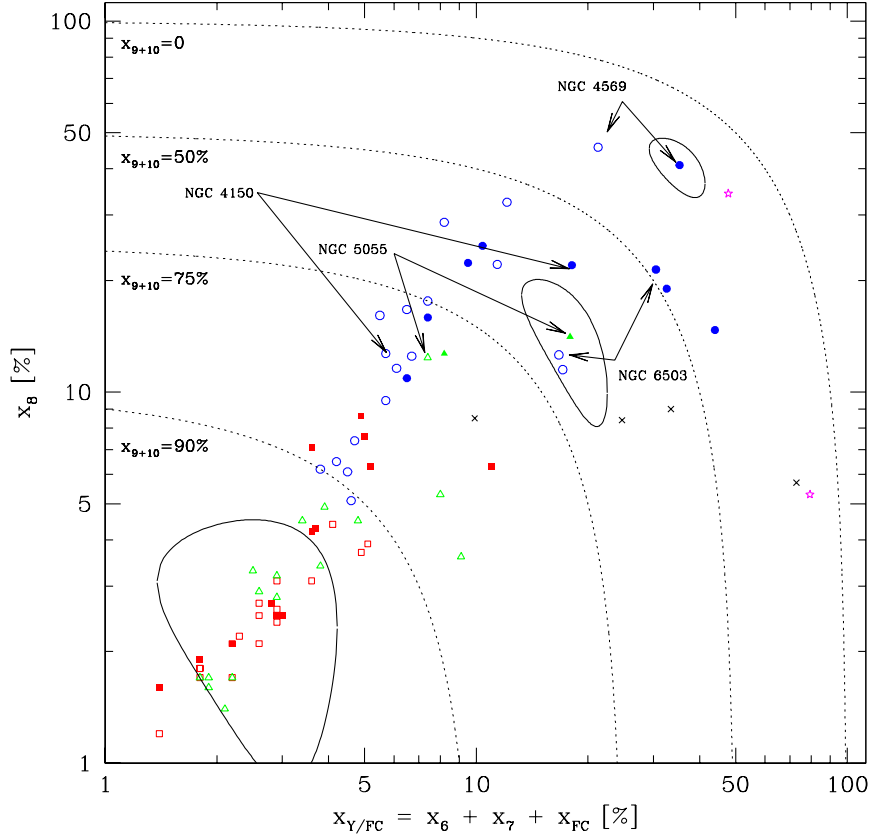


Fig. 13.— 2D projection of the EPS results. The young plus FC component is in the horizontal axis and the 10^8 yr stellar component in the vertical axis. A third perpendicular axis carries the remaining fraction of the flux, which goes in stars of 10^9 yr or more. Dotted lines represent the loci of constant $x_9 + x_{10}$. Different symbols represent different η classes of LLAGN, as in Figure 9. Arrows mark the position of several LLAGN that have been observed from the ground (open symbols) and with STIS (filled symbols), and they show the variation of the stellar population due to the aperture effect. Ellipses show the uncertainties associated to three representative points: NGC 4569 ($x_{Y/FC} = 35 \pm 6$ %, $x_8 = 41 \pm 7$ %); NGC 5055 ($x_{Y/FC} = 18 \pm 5$ %, $x_8 = 14 \pm 6$ %); and NGC 7331 ($x_{Y/FC} = 3 \pm 1$ %, $x_8 = 3 \pm 2$ %). Error ellipses have been computed using the errors and their covariances according to the expressions given by: <http://laeff.inta.es/users/mcs/SED/Theory/slide8.html>

5.4. Comparison with Seyfert 2s: The role of starbursts in LLAGN

Our previous investigations of the stellar populations in type 2 Seyferts provide an interesting reference for comparison. Powerful circumnuclear starbursts have been unambiguously identified in $\sim 40\%$ of nearby Seyfert 2s (Heckman et al 1997; González Delgado et al 1998; Storchi-Bergmann et al 1998; González Delgado, Heckman & Leitherer 2001; Joguet et al 2001). These starbursts were originally detected by means of either UV imaging, UV spectroscopy or the WR bump. Among other galaxy properties, these starbursts affect the equivalent width of the CaII K line, which becomes diluted to $W_K < 10 \text{ \AA}$ (Cid Fernandes et al 2001a). Emission line ratios are also affected. While in “pure Seyfert 2s” (defined as nuclei with no clear signs of starburst activity) line ratios like HeII/H β and [OIII]/H β assume a wide range of values, composite systems have systematically lower values of these ratios. The interpretation is straightforward. Since photoionization by a starburst contributes more to H β than to typical Seyfert 2 lines like HeII λ 4686 and [OIII] λ 5007, the presence of a starburst around a Seyfert 2 nucleus has the effect of diluting HeII/H β and [OIII]/H β with respect to the pure AGN values. The resulting line ratios are in between those of starbursts and “pure Seyfert 2s”. In Cid Fernandes et al (2001a) and Storchi-Bergmann et al (2001) we further speculated that composite starburst + Seyfert 2 systems evolve into “pure Seyfert 2s”.

The analogies with the results reported in this paper are evident. Our stellar-LLAGN, i.e. LLAGN with HOBLs, diluted metal absorption lines and low [OI]/H α , qualitatively resemble starburst + Seyfert 2 composites. Similarly, LLAGN with predominantly old stellar populations, are analogous to “pure Seyfert 2s”. In broad terms, the results reported in this paper sound like a low luminosity extension of the starburst-AGN connection identified in Seyfert 2s.

These similarities suggest that LLAGN with HOBL harbor a starburst. But do they? Undoubtedly, the most remarkable result of our survey is that HOBLs are ubiquitous, if not omnipresent, in weak-[OI] LLAGN. The problem is that HOBLs are not direct signposts of ongoing star-formation. Instead, they signal the presence of 10^8 – 10^9 yr populations (González Delgado et al 2001). It is useful to recall here that for Seyfert 2s we have found that in all cases where young stars have been conclusively detected by UV data (Heckman et al 1997; González Delgado et al 1998), HOBLs are present in the optical. In other words, every time a young, $< 10^7$ yr starburst is seen in the UV, a $\gtrsim 10^8$ yr population is identified in the optical by its deep HOBLs, which points to multiple bursts or \sim continuous star-formation regime. Inverting and extrapolating from this result, the ubiquity of HOBLs in weak-[OI] LLAGN could thus be interpreted as indirect evidence for the existence of young stars, which, as pointed out above, naturally explains the distribution of points in our [OI]/H α versus W_λ and x_O diagrams. However, when young starbursts are present in

LLAGN, they are generally faint (see Table 3 and 4). The fact that low luminosity AGN are associated with low luminosity starbursts may be a trivial consequence of a “starburst \propto AGN” scaling law, which might exist for the mere reason that both starbursts and super massive black-holes feed on gas. As pointed out by Ho, Filippenko, & Sargent (2003), the gaseous content of LINERs and TOs is small compared to that of Seyferts, which can potentially explain why starbursts are more easily found in Seyfert 2s than in LLAGN.

Further insight can be gained by comparing the EPS of LLAGN to results obtained in previous investigations. In Figure 14b we plot the EPS of 35 Seyfert 2s from Cid Fernandes et al (2001a, renormalized to $\lambda = 4020 \text{ \AA}$). Similarly, in Figure 14c we plot the results for 57 Starburst and HII galaxies from Cid Fernandes et al (2003b). Filled and open symbols in Figure 14b represent respectively starburst + Seyfert 2 composite systems and “pure Seyfert 2s”. “Pure Seyfert 2s” are less luminous than composites, and comprise both objects dominated by old stars and sources which present an excess blue continuum whose nature we cannot ascertain with confidence (Storchi-Bergmann et al 2000). The most likely sources for this blue continuum are scattered light from the AGN and a relatively weak starburst.

Two differences stand out when comparing LLAGN with Seyfert 2s. First, young starbursts appear far more frequently in Seyfert 2s. For instance, $\sim 40\%$ of Seyfert 2s but less than 10% of the LLAGN are located above the $x_{9+10} = 50\%$ line⁴. In fact, most of the starburst + Seyfert 2 composites populate the same region as *bona fide* starburst galaxies (Figure 14c). Further evidence that young stars are more easily detected in Seyfert 2s than in LLAGN is that whereas the WR bump has been detected in $\sim 10\%$ of the Seyfert 2s in the samples of Cid Fernandes et al (2001a) and Joguet et al (2001), we have not detected this feature in any of our LLAGN. This does *not* imply that LLAGN lack young massive stars altogether. After all, we know from our analysis and UV work (Maoz et al 1998; Colina et al. 2002) that at least some LLAGN contain these stars. Their relative contribution to the optical flux, however, is clearly much less relevant than in Seyfert 2s. Given the similarities in the host galaxy properties of Seyferts, LINERs and TOs, this result implies that starbursts around LLAGN are generally weaker than in Seyfert 2s.

Secondly, Seyfert 2s are visibly more spread out than LLAGN in our evolutionary diagram. Interpreted in terms of stellar populations alone (i.e. neglecting the effects of scattered light), this result implies that Seyfert 2 have more mixed stellar populations due to stronger and/or more numerous starbursts in the recent ($\sim 10^8$ yr) past. The strong clustering of LLAGN along the evolutionary tracks for ages $\gtrsim 1$ Gyr is simply not seen for Seyfert 2s.

⁴Note, however, that we can not exclude here that this difference could be due to a circumnuclear starburst (100-500 pc) in Seyfert 2 galaxies, instead of young stars in the central 100 pc.

5.5. Speculations on an evolutionary scenario

It is further tempting to speculate that at least some Seyfert 2s evolve into LLAGN. The intense star-formation in Seyfert 2 composites must eventually cease with the continuous consumption of the gas supply. Barring further fuelling events (e.g. interactions), passive evolution of the stellar populations would move these Seyfert 2s roughly along evolutionary paths between the pure IB and $c_O = 40\%$ models in Figure 14a, which leads to LLAGN. If star-formation gradually decays on time-scales of $\sim 10^8$ yr (instead of ceasing abruptly), after $\sim 10^8$ yr a strong post-starburst (with pronounced HOBLs) would coexist with an incipient young population. This is the basic stellar mixture found in the TOs above the $c_O < 40\%$ track in Figure 14a. Concomitantly, the UV–blue continuum and emission line luminosities of the system would decrease steadily because of the drop in star-formation and accretion rates as gas becomes less and less available. Luminosities in the red should change less because of the steady output from the underlying old bulge population. At ~ 1 Gyr these systems would reach the “turn-over” at $x_{Y/FC} \sim 10$ and $x_8 \sim 30\%$ in Figure 14. HOBLs from $\sim 10^9$ yr populations would be present. Young stars, if present, should contribute little to the optical continuum and thus be hard to detect. In another Gyr or so they would reach the $x_{9+10} \gtrsim 90\%$ zone occupied by $\eta = O$ sources. The gas excitation in this phase would presumably be dominated by the AGN, which is consistent with the fact that strong-[OI] sources are exclusively found in this region. The relative durations of these phases would become progressively longer along the evolutionary sequence, which seems to be quantitatively consistent with the demographics of Seyfert 2s and LLAGN.

One can start this evolution from other initial positions in Figure 14, although $c_0 \gtrsim 40\%$ is required to turn a composite Seyfert 2 into $\eta = I$ TOs (compare Figure 14a and b). The “pure Seyfert 2s” between $x_{Y/FC} = 10$ and 50% in Figure 14b could well skip the $\eta = I$ phase altogether and move directly to $\eta = I/O$ or O LLAGN. Young stars, if present, would play an irrelevant role in the gas all the way along this sequence. The change from high to low excitation emission line-ratios, i.e. from Seyfert 2 to LINER, would be attributed to changes in the accretion rate. In summary, Seyfert 2s contain more younger starbursts than LLAGN.

6. Summary and Conclusions

This is the second paper in a series that deals with the study of the stellar populations in LLAGN. The goal is to determine whether the stellar populations in the central 20-100 pc of these galaxies are related with the ionization processes of the nuclear gas. For this goal, we have collected STIS optical (2900-5700 Å) spectra of 28 LLAGN plus 4 HII nuclei and 1

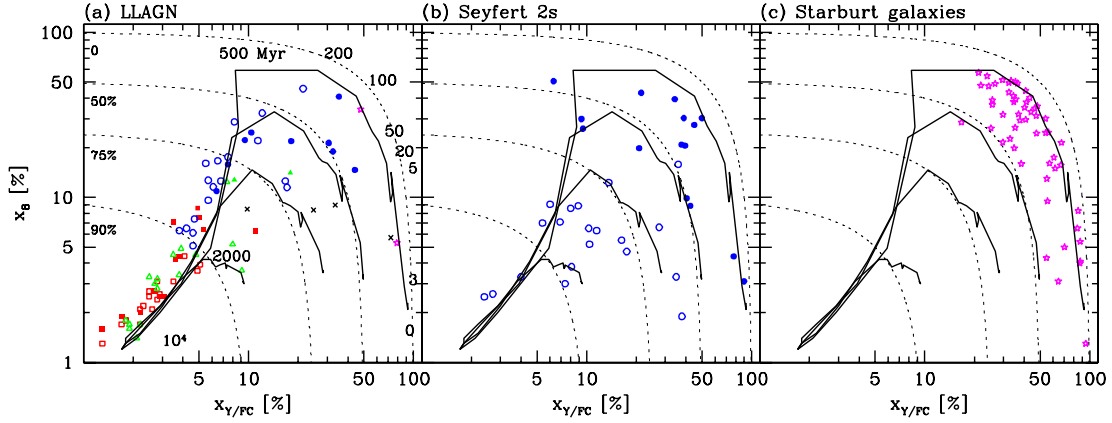


Fig. 14.— Comparison of the EPS results of LLAGN (panel *a*), Seyfert 2s (*b*) and Starburst galaxies (*c*) in our “evolutionary diagram”. Dotted lines in all panels mark contours constant x_{9+10} , as labelled in the left of panel *a*. Symbols in panel *a* are as in Figure 13. Solid lines trace the evolution of an instantaneous burst (IB) in this EPS diagram. Labels along the outer evolutionary line in panel *a* indicate the age (in Myr). The four different lines correspond to different contrast ratios c_0 of the burst to an underlying 15 Gyr old population. The outer line correspond to $c_0 = 0\%$, ie, a pure burst, while the inner lines correspond to $c_0 = 40, 60$ and 80% from right to left. These fractions refer to the time when the burst starts.

non-active galaxy from the HST archive. These data are added to the ground-based spectra of the LLAGN presented in Paper I. In total, we have analyzed a sample of 73 LLAGN, which represents 45% of this type of objects in the HFS97 catalogue. In this second paper we have (1) described the sample; (2) classified the STIS nuclear (0.2×1 arcsec) stellar population by comparing with normal galaxies; (3) measured the equivalent widths and colors indicative of the stellar populations; (4) performed stellar population synthesis (EPS) of the whole sample; (5) correlated EPS results with the emission line ratio $[\text{OI}]/\text{H}\alpha$. LLAGN are divided according with their $[\text{OI}]/\text{H}\alpha$ ratio in two subtypes: strong- $[\text{OI}]$ ($[\text{OI}]/\text{H}\alpha \geq 0.25$) and weak- $[\text{OI}]$ ($[\text{OI}]/\text{H}\alpha \leq 0.25$). The main results are summarized below:

1. Weak- $[\text{OI}]$ LLAGN present a higher contribution of the intermediate age population than strong- $[\text{OI}]$. They also seem to have a younger stellar population on average.
2. The relation between $[\text{OI}]/\text{H}\alpha$ and the stellar population suggests a stellar origin for the ionization of weak- $[\text{OI}]$ LLAGN with HOBL in absorption, although the contribution of massive stars is small in the aperture of the ground-based spectra.
3. On the other hand, STIS spectra show a larger contribution of young stars in the case of weak- $[\text{OI}]$ LLAGN than in the ground-based data, suggesting that its reduced contribution is an effect of the lower contrast of the ground-based data. This result suggests that the dominant source in weak- $[\text{OI}]$ LLAGN with an intermediate age population is thus stellar. This is confirmed by the HST UV spectra available for a few objects.
4. On the other hand, the dominant source of ionization in strong- $[\text{OI}]$ LLAGN is likely an AGN, which is consistent with the detection of broad Balmer lines in emission in a few cases and a larger contribution of older stars to their stellar population.
5. Evolutionary models for the stellar population suggest an age sequence in which the weak- $[\text{OI}]$ LLAGN are younger objects than the strong- $[\text{OI}]$. The evolution proceeds as the small starburst in the nuclei of the weak- $[\text{OI}]$ fades away decreasing the stellar contribution to the intensity of $\text{H}\alpha$ and leading to a larger $[\text{OI}]/\text{H}\alpha$ ratio.
6. The evolutionary scenario proposed here is similar to the one we have previously proposed for Seyfert 2 galaxies (Storchi-Bergmann et al. 2001, Cid Fernandes et al. 2001a), in which a Seyfert 2 with a circumnuclear starburst (composite Seyfert 2) evolves to a "pure" Seyfert 2 as the starburst fades. The weak- $[\text{OI}]$ LLAGN seem to be lower luminosity counterparts of composite Seyfert 2 galaxies, while the strong- $[\text{OI}]$ LLAGN would be the pure LINERs. The difference between the Seyfert 2 and LINERs would be mainly due to the smaller accretion rate or efficiency in LINERs.

Acknowledgments

We thank Grazyna Stasińska, Miguel Cerviño, and Luis Colina their helpful comments from a through reading of the paper, and the referee for her/his suggestions that help to improve the paper. RGD, and EP acknowledge support by the Spanish Ministry of Science and Technology (MCyT) through grants AYA-2001-3939-C03-01 and AYA-2001-2089. RCF and TSB acknowledge the support from CNPq and CAPES. Some of these data are from observations made with the NASA/ESA Hubble Space Telescope, obtained from the data archive at the ST-ECF. Additional data presented here have been taken using ALFOSC, which is owned by the Instituto de Astrofísica de Andalucía (IAA) and operated at the Nordic Optical Telescope under agreement between IAA and the NBIfAFG of the Astronomical Observatory of Copenhagen. We are grateful to the IAA director for the allocation of 5.5 nights of the ALFOSC guaranteed time for this project.

REFERENCES

- Balogh, M. L., Morris, S. L., Yee, H. K. C., Carlberg, R. G., Ellingson, E. 1999, *ApJ*, 527, 54
- Barth, A. & Shields, J. C. 2000, *PASP*, 112, 753
- Bica, E.& Alloin, D. 1983a, *A&AS*, 66, 171
- Bica, E.& Alloin, D. 1983b, *A&A*, 162, 21
- Binette, L., Magris, C. G., Stasinska, G., Bruzual, A. G. 1994, *A&A*, 292, 13
- Bruzual, G. & Charlot, S. 1993, *ApJ*, 405, 538
- Cid Fernandes, R. & Terlevich, R. 1995, *MNRAS*, 272, 423
- Cid Fernandes, R., Heckman, T., Schmitt, H., González Delgado, R. M., Storchi-Bergmann, T. 2001a, *ApJ*, 558, 81
- Cid Fernandes, R., Sodr e, L., Schmitt, H., & Leão, J. R. S. 2001b, *MNRAS*, 325, 60
- Cid Fernandes, R., Leão, J. R. S. & Rodrigues-Lacerda, R. 2003b, *MNRAS*, 340, 29
- Cid Fernandes, R., González Delgado, R.M., Schmitt, H., Storchi-Bergmann, T., Pires, L., Pérez, E., Heckman, T., Leitherer, C., & Schaerer, D. 2003a, *ApJ*, submitted (Paper I)
- Colina, L., González Delgado, R.M., Mas-Hesse, J.M., Leitherer, C. & Jiménez-Bailón, E. 2002, 579, 545
- Filippenko, A.V. & Terlevich, R. 1992, *ApJ*, 397, L79
- Filippenko, A.V. 1996, *ASP Conf. Series*, 103, 17

- González Delgado, R.M., Heckman, T. Leitherer, C., Meurer, G., Krolik, J., Wilson, A.S., Kinney, A. & Koratkar, A. 1998, ApJ, 505, 174
- González Delgado, R.M., Leitherer, C. & Heckman, T.M. 1999, ApJS, 125, 489
- González Delgado, R.M. Heckman, T.M. & Leitherer, C. 2001, ApJ, 546, 845
- González Delgado, R.M., et al. 2003, ASP conf., 297, 417
- Heckman, T.M., González Delgado, R.M., Leitherer, C., Meurer, G., Krolik, J., Kinney, A., Koratkar, & Wilson, A.S. 1997, ApJ, 482, 114
- Ho, L.C., Filippenko, A.V. & Sargent, W.L.W. 1997a, ApJS, 112, 315
- Ho, L.C., Filippenko, A.V. & Sargent, W.L.W. 1997b, ApJS, 112, 391
- Ho, L.C., Rudnick, G., Rix, H-W., Shields, J.C., McIntosh, D. H., Filippenko, A.V., Sargent, W.L.W., & Eracleous, M. 2000, 541, 120
- Ho, L. C. et al. 2001, 549, L51
- Ho, L.C., Filippenko, A.V. & Sargent, W.L.W. 2003, ApJ, 583, 159
- Jiménez-Bailón, E., Satos-Leó, M., Mas-Hesse, J.M., Guainazzi, M., Colina, L., Cerviño, M., González Delgado, R.M. 2003, ApJ, in press
- Joguet, B., Kunth, D., Melnick, J., Terlevich, R., & Terlevich, E. 2001, A&A, 380, 19
- Kauffmann, G., et al 2003, MNRAS, 341, 54
- Maoz, D., Koratkar, A., Shields, J. C., Ho, L. C., Filippenko, A. V., & Sternberg, A. 1998, AJ, 116, 55
- Pogge, R.W., & Martini, P. 2002, ApJ, 569, 624
- Raimann, D., Storchi-Bergmann, T., Gonzalez Delgado, R. M., Cid Fernandes, R., Heckman, T., Leitherer, C., Schmitt, H. 2003, MNRAS, 339, 772
- Schmidt, A.A., Copetti, M.V.F., Alloin, D., & Jablonka, P. 1991, MNRAS, 249, 766
- Schmitt, H.R., Storchi-Bergmann, T., & Cid Fernandes, R. 1999, MNRAS, 303, 173
- Shields, J.C. 1992, ApJ, 399, L27
- Shields, J.C., Rix, H-W., McIntosh, D. H., Ho, L.C., Rudnick, G., Filippenko, A.V., Sargent, W.L.W., & Sarzi, M. 2000, 541, 120
- Smith, L.J., Norris, R.P.F., & Crowther, P.A. 2002, MNRAS, 337, 1309
- Stasinska, G. 1984, A&A, 135, 341
- Storchi-Bergmann, T., Eracleous, M., Ruiz, M.T., Livio, M., & Wilson, A.S., Filippenko, A. V. 1997, ApJ, 489, 87

- Storchi-Bergmann, T., Cid Fernandes, R., & Schmitt, H. R. 1998, *ApJ*, 501, 94
- Storchi-Bergmann, T., Raimann, D., Bica, E. L. D. & Fraquelli, H. A. 2000, *ApJ*, 544, 747
- Storchi-Bergmann, T., González Delgado, R. M., Schmitt, H. R., Cid Fernandes, R., & Heckman, T. 2001, *ApJ*, 559, 147
- Taniguchi, Y., Shioya, Y., & Murayama, T. 2000, *AJ*, 120, 1265
- Terashima, Y., Ho, L.C., & Ptak, A.F. 2000, *ApJ*, 539, 161
- Terlevich, R., & Melnick, J. 1985, *MNRAS*, 213, 841
- Worthey, G. & Ottaviani, D. L. 1997, *ApJS*, 111, 377